1240174
(0075142H)

RPP-RPT-49288, Rev. 0

C Farm Surface Geophysical Exploration-Reprocessing

Prepared by **Dale Rucker, hydroGEOPHYSICS, Inc.** for
Washington River Protection Solutions, LLC
Richland, WA 99352
U.S. Department of Energy Contract DE-AC27-08RV14800

RECEIVED
SEP 13 2016
EDMC

EDT/ECN: DRF UC:
Cost Center: Charge Code:
B&R Code: Total Pages: 72

Key Words: SGE, surface geophysical exploration, C tank farm

Abstract: A reanalysis of data taken during an electrical resistivity survey in 2006 was conducted at the C tank farm to evaluate the spatial distribution of subsurface electrical properties associated with past releases. Several tanks, waste transfer lines, spare inlet valves, and unplanned releases have released waste to the subsurface. It was anticipated that the resistivity method, using wells as long electrodes and surface electrodes placed along the periphery of the farm, could image the locations of these releases. The results showed a major electrical resistivity target beneath the SST C-101. Other minor targets were also found that should be investigated further.

TRADEMARK DISCLAIMER. Reference herein to any specific commercial product, process, or service by trade name, trademark, manufacturer, or otherwise, does not necessarily constitute or imply its endorsement, recommendation, or favoring by the United States Government or any agency thereof or its contractors or subcontractors.

MAY 24 2011
DATE:
STA: 15
HANFORD RELEASE
ID:
65

Nancy A Fouad 5/24/2011
Release Approval Date Release Stamp

Approved For Public Release

EXECUTIVE SUMMARY

A reanalysis of data taken an electrical resistivity survey in 2006 was completed at the C tank farm on the Hanford Site. Two types of electrodes were used in the survey: surface electrodes placed along lines on the periphery of the tank farm and long electrodes (i.e., wells) distributed among the tanks and around the tank farm. The wells as long electrodes were completed to depths from 15 to 94 meters below ground surface. The two types of electrodes produced three datasets, including surface electrode-to-surface electrode, well-to-surface-electrode, and well-to-well. All three datasets were inverse modeled together with software that can accommodate both the surface and long electrodes.

The results of the inverse modeling done in the reanalysis showed a prominent low resistivity feature beneath SST C-101. Figure ES-1 shows the resistivity distribution for the uppermost layer of the model, with the target beneath SST C-101 showing up as having the lowest resistivity values. Several other low resistivity features appeared in the model including the diffuse target that is near UPR-82, which is presently being investigated as part of another Surface Geophysical Exploration project. Results of the UPR-82 model should be completed by September 2011. Targets are also seen at SST C-105, SST C-107, beneath SST C-104, and south of SST C-103. Not shown is a potentially deeper target that exists beneath SST C-108. The target beneath SST C-108 is not connected to the surface and its source is unknown.

Figure ES-1. Resistivity Results of the Uppermost Layer for the C Tank Farm Model.

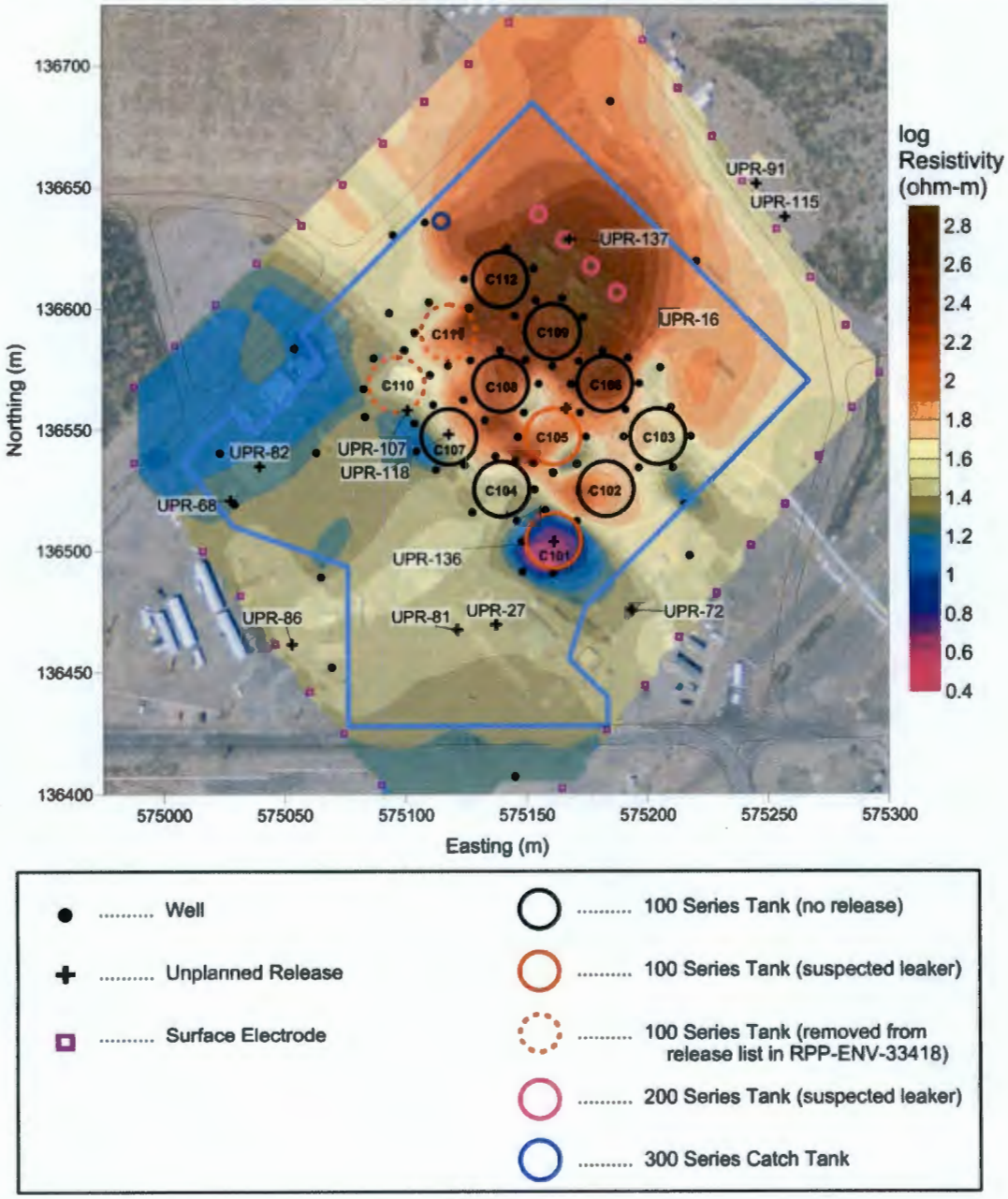

TABLE OF CONTENTS

1.0 INTRODUCTION 1-1
- 1.1 SCOPE 1-3
- 1.2 OBJECTIVES 1-4
- 1.3 REPORT LAYOUT 1-4

2.0 BACKGROUND 2-1
- 2.1 SITE DESCRIPTION 2-1
- 2.2 SUMMARY OF HYDROGEOLOGIC CONDITIONS 2-1
- 2.3 TANK CONTENTS 2-5
- 2.4 UNPLANNED RELEASES AT OR NEAR C TANK FARM 2-6
- 2.5 PAST CHARACTERIZATION OF C FARM 2-7

3.0 DATA ACQUISITION—WELL-TO-WELL SURVEY 3-1
- 3.1 SURVEY AREA AND COVERAGE 3-1
  - 3.1.1 Surface-to-Surface Data Acquisition 3-1
  - 3.1.2 Well-to-Surface and Depth Electrode-to-Surface Data Acquisition 3-4
  - 3.1.3 Well-to-Well and Well-to-Depth Electrode Data Acquisition 3-4
- 3.2 INSTALLATION AND SETUP 3-5
  - 3.2.1 Installation of Remote Reference Arrays 3-7
  - 3.2.2 Permanent Surface Electrodes 3-7
  - 3.2.3 Resistivity Equipment 3-8
- 3.3 RECIPROCAL DATA COLLECTION 3-8

4.0 MODELING RESULTS 4-1
- 4.1 NEW MODELING RESULTS 4-1
- 4.2 SUMMARY OF PAST MODELING RESULTS 4-11

5.0 CONCLUSIONS 5-1

6.0 REFERENCES 6-1

LIST OF APPENDICES

A QUALITY ASSURANCE ..... A-i

B THEORY ..... B-i

LIST OF FIGURES

1-1. Location of C Tank Farm and other Tank Farms on the Hanford Site. 1-2

1-2. C Tank Farm Area Showing Geophysical Survey Layout Showing the Locations of Wells and Surface Electrodes Used for the Analysis. 1-3

2-1. Location Map of Waste Management Area C and Surrounding Area and Cross-Section Lines shown in Figure 2-2. 2-2
2-2. Subsurface Conditions in Vicinity of Waste Management Area C. 2-3
2-3. Nitrate Concentrations (milligrams/liter) Measured in Ground Water Around C Tank Farm – June 2005 2-7
2-4. Results of Spectral Gamma Characterization of Drywells in C Farm, for Cesium-137 and Cobalt-60. 2-9
2-5. Electrical Conductivity (EC) Measurements in Porewater Extracted from Soil Samples Taken around C Farm. 2-11
3-1. Location of Drywells, Groundwater Wells, and Buried Electrodes Used for Surface Geophysical Exploration Survey. 3-2
3-2. Forward Pole-Pole Electrode Measurement. 3-5
3-3. Schematic of Reverse Pole-Pole Electrode Measurements. 3-5
3-4. Field Setup and Equipment for the Well-to-Surface Survey. 3-6
3-5. Field Worker Attaching Wire to Well. 3-7
3-6. Scatter of WTW Transfer Resistance Data from WMA C. 3-8
3-7. Scatter of WTS Transfer Resistance Data from WMA C. 3-9
3-8. Scatter of STS Transfer Resistance Data from WMA C. 3-10
4-1. Transfer Resistance Versus Distance Data Used in the Inverse Model. 4-2
4-2. Plan View Slice (Uppermost Layer at 0.5 m) of Calculated Resistivity for Model CFarm_006. 4-4
4-3. Three-dimensional View of a Low Resistivity Target Beneath C Tank Farm, View from Southeast to Northwest for Model CFarm_006. 4-5
4-4. Three-dimensional View of a Low Resistivity Targets Beneath C Tank Farm, Plan View (Top) and View Looking East (Bottom). 4-6
4-5. Plan View Slice (Uppermost Layer at 0.5 m) of Calculated Resistivity with Spectral Gamma Data Collected in Dry Wells. 4-8
4-6. Plan View Slice (Uppermost Layer at 0.5 m) of Calculated Resistivity with Electrical Conductivity Data Collected at selected Direct Push Locations. 4-10
4-7. Map of C Farm Showing WTW Inversion Modeling Domains (from RPP-RPT-31588). 4-12
4-8. WTW Inversion Results using Drywells Only (from RPP-RPT-31588). 4-13

LIST OF TABLES

2-1. General Groundwater Flow Directions and Flow Rates for Single-Shell Tank Waste Management Area C in the 200 East Area 2-5
3-1. Summary of Data Coverage. 3-3
3-2. Dry Wells and Groundwater Wells Used for Surface Geophysical Exploration Survey. (2 Sheets) 3-3
4-1. Inverse Modeling Data File Statistics 4-2

LIST OF TERMS

Abbreviations and Acronyms

3D	three dimensional
DOE	U.S. Department of Energy
EC	electrical conductivity
HFFACO	*Hanford Federal Facility Agreement and Consent Order*
HRR	high resolution resistivity
PUREX	plutonium-uranium extraction
RCRA	*Resource Conservation and Recovery Act of 1976*
RMS	root-mean-square
SGE	Surface Geophysical Exploration
SST	single-shell tank
STS	surface-to-surface
UPR	unplanned release
WMA	waste management area
WRPS	Washington River Protection Solutions, LLC
WTD	well-to-depth electrode
WTS	well-to-surface
WTW	well-to-well

Units

cm	centimeter
ft	foot
g	gram
gal	gallon
in.	inch
kg	kilogram
L	liter
m	meter
mS	milliSiemen
µg	microgram
ohm-m	resistances* meters
pCi	picocurie

1.0 INTRODUCTION

This report presents the results of a reanalysis (including data reduction, processing, and inversion) of electrical resistivity data collected during an investigation of the Waste Management Area C tank farm (C farm) and surrounding areas for subsurface contamination at the U.S. Department of Energy's (DOE) Hanford Site in Washington State (Figure 1-1). The original C tank farm resistivity project was conducted in 2006 and the results were reported in RPP-RPT-31558, *Surface Geophysical Exploration of C Tank Farm*. The current scope includes a reanalysis of the original data to make use of advances in Surface Geophysical Exploration (SGE) computing capability and software that have been implemented since 2005. This investigation was specifically designed to apply both new analytical software and hardware to C farm resistivity data and to provide an assessment of the changes, if any, in the analysis of C farm resistivity anomalies.

The 2006 C farm survey included a pole-pole array incorporated in the high resolution electrical resistivity data collected using (1) the well-to-well (WTW) methodology with existing groundwater and vadose zone wells; (2) surface-to-surface (STS) collected on four lines using surface electrodes located along the periphery of the C farm fence; and (3) a combined well-to-surface (WTS) where the wells and surface electrodes were collected in a joint acquisition survey. Figure 1-2 shows a layout of the various wells and electrodes used in the survey. This current work scope was performed for Washington River Protection Solutions, LLC, (WRPS) to investigate potential contamination from the tank farm and the surrounding areas. The overall objective of the survey was to map low resistivity anomalies associated with unplanned releases that can be evaluated as potential areas of contamination from past leaks and spills.

For the original resistivity analysis conducted in 2006, it was necessary to parse the data into subareas for individual data processing, and then stitch the resulting information back together to form a complete image of the subsurface. The approach, while necessary at the time due to hardware and software limitations, can result in errors at the boundaries causing mismatch between adjacent model domains, thus impacting the final analysis (Rucker et al. 2009). In contrast, the present analysis uses all information together in one large domain in hopes of avoiding the boundary mismatch issue. Additionally, lessons learned from previous SGE projects at the Hanford Site regarding noise and potentially bad data from measurement errors, were applied to the raw C farm data in order to formulate a new processed data set ready for inversion.

Figure 1-1. Location of C Tank Farm and other Tank Farms on the Hanford Site.

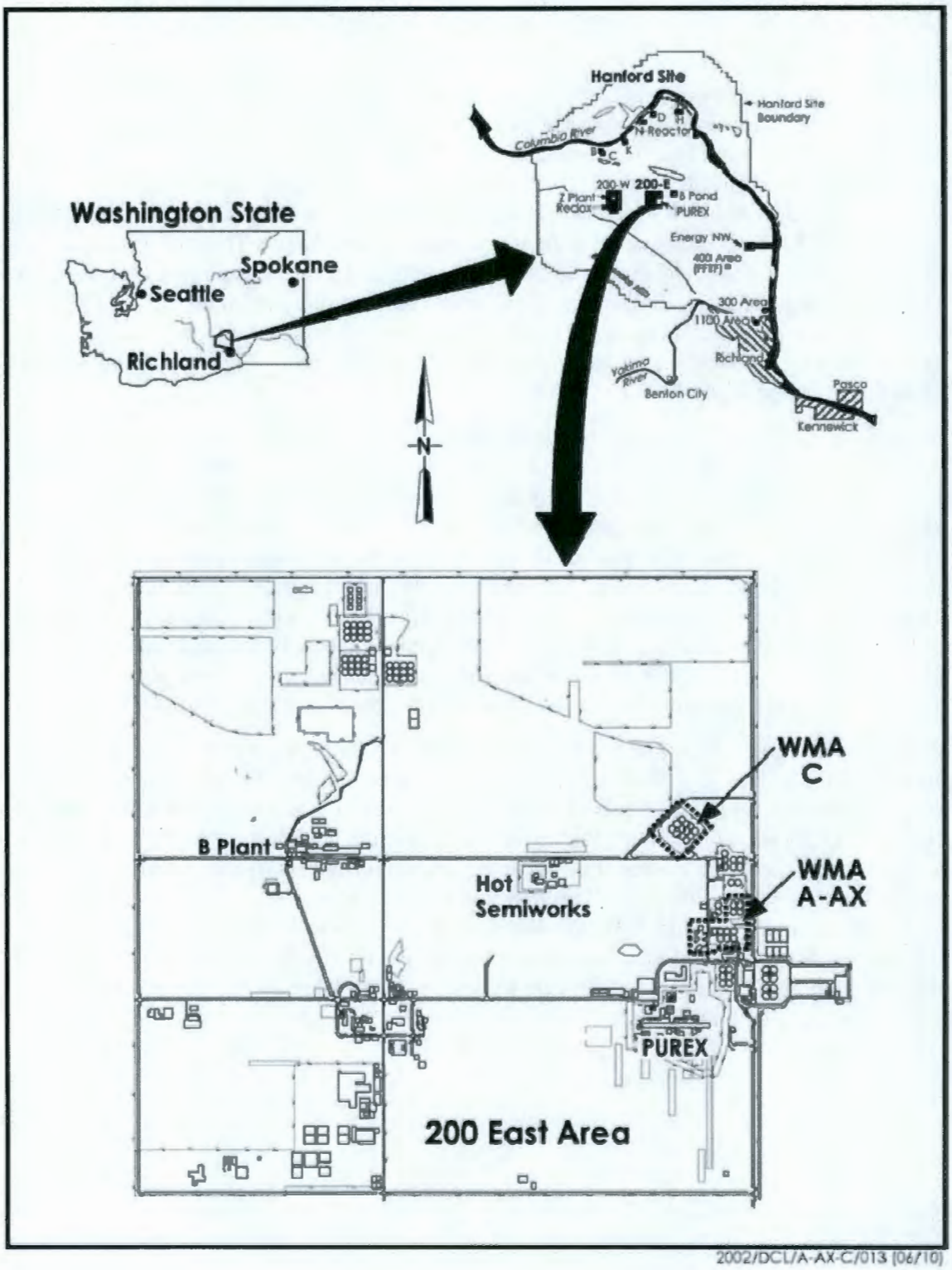

2002/DCL/A-AX-C/013 (06/10)

Figure 1-2. C Tank Farm Area Showing Geophysical Survey Layout Showing the Locations of Wells and Surface Electrodes Used for the Analysis.

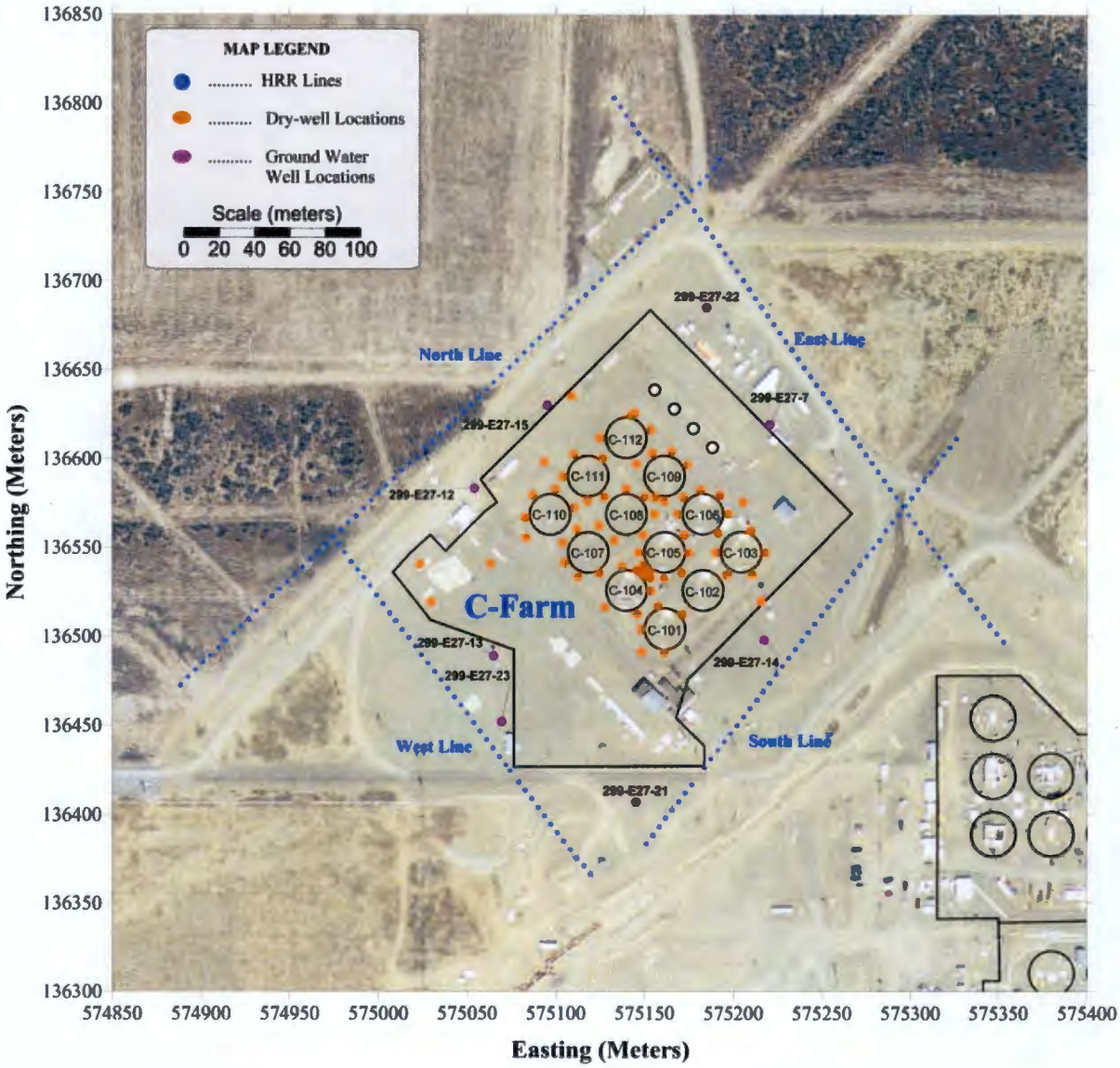

1.1 SCOPE

The scope of this project was to provide an assessment of the changes, if any, in the analysis of C farm resistivity anomalies using the latest generation of computer hardware and software designed explicitly to model large electrical resistivity datasets. The re-analysis included resistivity data from the vadose zone and groundwater wells within and around C tank farm, and data collected on surface electrodes on the periphery of the tank farm fence.

1.2 OBJECTIVES

The main objective of the current work was to reprocess the original C farm data acquired in 2006 using the new algorithms, processing methodologies, different acquisition modalities, and computing platforms available to current SGE projects.

1.3 REPORT LAYOUT

The overall scope and content of this report is divided into several main sections as follows:

- **Section 1.0, Introduction** – Describes the scope and objectives of the investigation.
- **Section 2.0, Background** – Provides a brief summary of the past history of C tank farm area including a brief discussion of the site geologic and hydrologic conditions.
- **Section 3.0, Data Acquisition** – Summarizes details of data acquisition of the survey
- **Section 4.0, Results and Interpretations** – Presents the results from the electrical resistivity surveying effort and an interpretation of the resistivity modeling results.
- **Section 5.0, Conclusions** – Provides a summary and conclusions drawn from the results and interpretations.
- **Appendix A, Quality Assurance** – Presents general methods and controls used to ensure the quality and control of data collection, reduction, and processing and configuration control of software and database changes used in this study.
- **Appendix B, Theory** – Presents the theory of resistivity acquired with the WTW method, WTS, and some modeling examples of targets to demonstrate sensitivity of the methods.

2.0 BACKGROUND

2.1 SITE DESCRIPTION

C farm is located in the Central Plateau, near the eastern edge of the 200 East Area (Figure 1-1). It was one of the first tank farms built, between 1944 and 1945. The tank farm contains twelve 100-series tanks, four 200-series tanks, and one 300-series catch tank (Figure 2-1). The 100-series tanks are 23 m (75 ft) in diameter, have a 5-m (15-ft) operating depth, and have an operating capacity of 2,006,000 L (530,000 gal) each. The 200-series tanks are 6 m (20 ft) in diameter with a 7.32-m (24-ft) operating depth and an operating capacity of 208,000 L (55,000 gal) each. The C-301 catch tank has a capacity of 136,000 L (36,000 gal). Only SSTs 241-C-101 (C-101) through 241-C-106 (C-106) have concrete pits. The other 100-series tanks are equipped with centrally located salt well pump pits. The tanks sit below grade with at least 2 m (7 ft) of soil cover to provide shielding from radiation exposure to operating personnel. Tank pits are located on top of the tanks and provide access to the tank, pumps, and monitoring equipment.

To support the transfer and storage of waste within waste management area (WMA) C single-shell tanks (SST), there is a complex waste transfer system of pipelines (transfer lines), diversion boxes, vaults, valve pits, and other miscellaneous structures.

Twelve unplanned releases (UPR) have occurred within or near C farm. The largest ones are associated with leaks in pipelines or diversion boxes, from inlet/outlet ports of the SSTs, or with leaks from the SSTs themselves. RPP-PLAN-39114, *Phase 2 RCRA Facility Investigation/Corrective Measures Study Work Plan for Waste Management Area C* provides more detail on these UPR sites. Six planned releases have also occurred within the tank farm, which include a septic discharge, drywells, and a French drain. Figure 2-1 shows the approximate location of all planned and unplanned releases.

Five SSTs (C-103, C-201, C-202, C-203, and C-204) have been retrieved to meet the requirements of *Hanford Federal Facility Agreement and Consent Order* (HFFACO) (Ecology et al. 1989). SST C-106 also has been declared retrieval complete (HNF-EP-0182, *Waste Tank Summary Report for Month Ending February 28, 2011*). Waste retrieval activities are currently ongoing and planned to complete waste retrieval from the remaining C farm tanks.

2.2 SUMMARY OF HYDROGEOLOGIC CONDITIONS

The hydrogeologic framework underlying WMA C and vicinity is well understood and is a result of several decades of site characterization activities that has been described in numerous reports (HW-61780, *Subsurface Geology of the Hanford Separation Areas;* ARH-LD-132, *Geology of the 241-C Tank Farm*; RPP-14430, *Subsurface Conditions Description of the C and A-AX Waste Management Area*; and RPP-35484, *Field Investigation Report for Waste Management Areas C and A-AX*).

Figure 2-1. Location Map of Waste Management Area C and Surrounding Area and Cross-Section Lines shown in Figure 2-2.

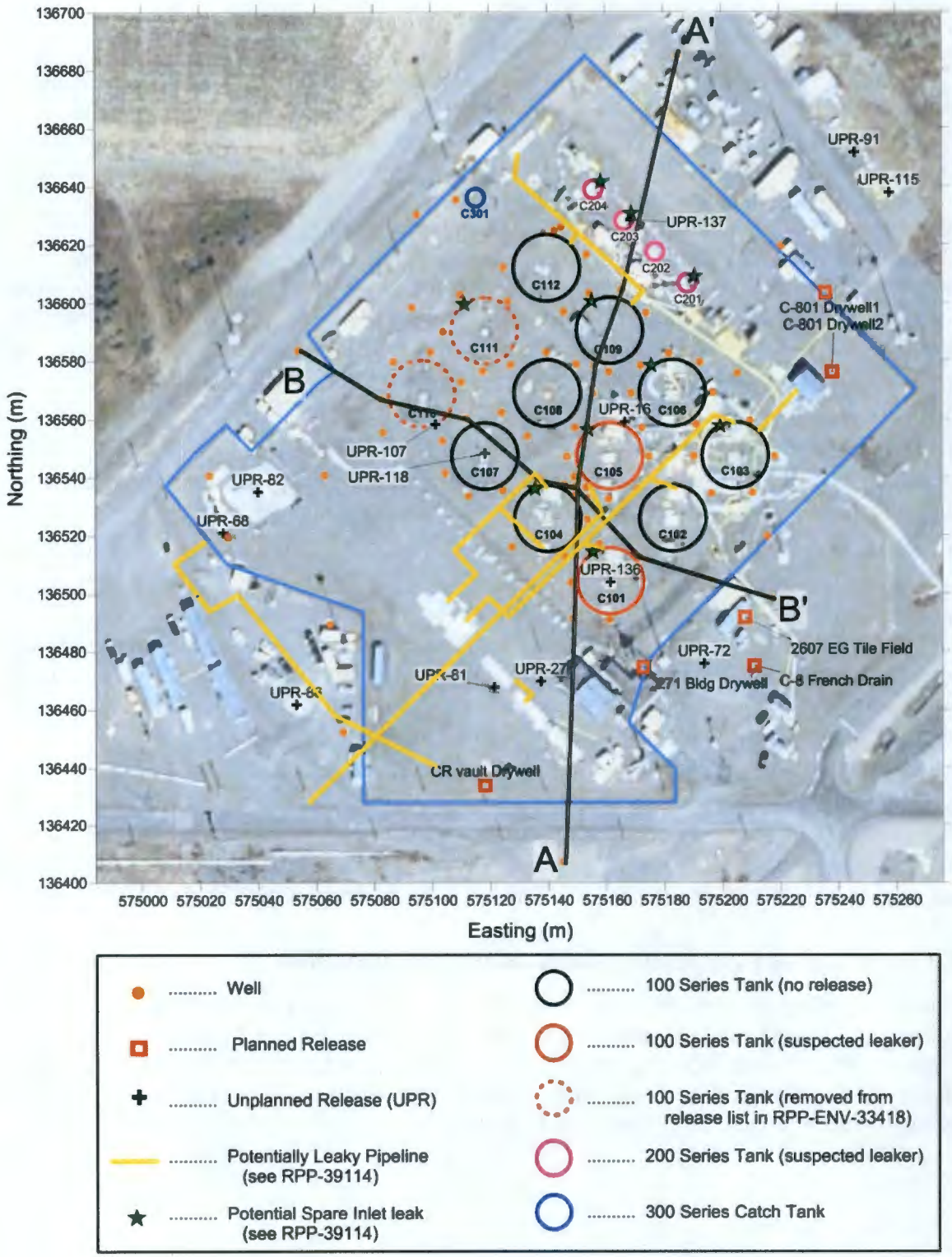

Figure 2-2. Subsurface Conditions in Vicinity of Waste Management Area C.

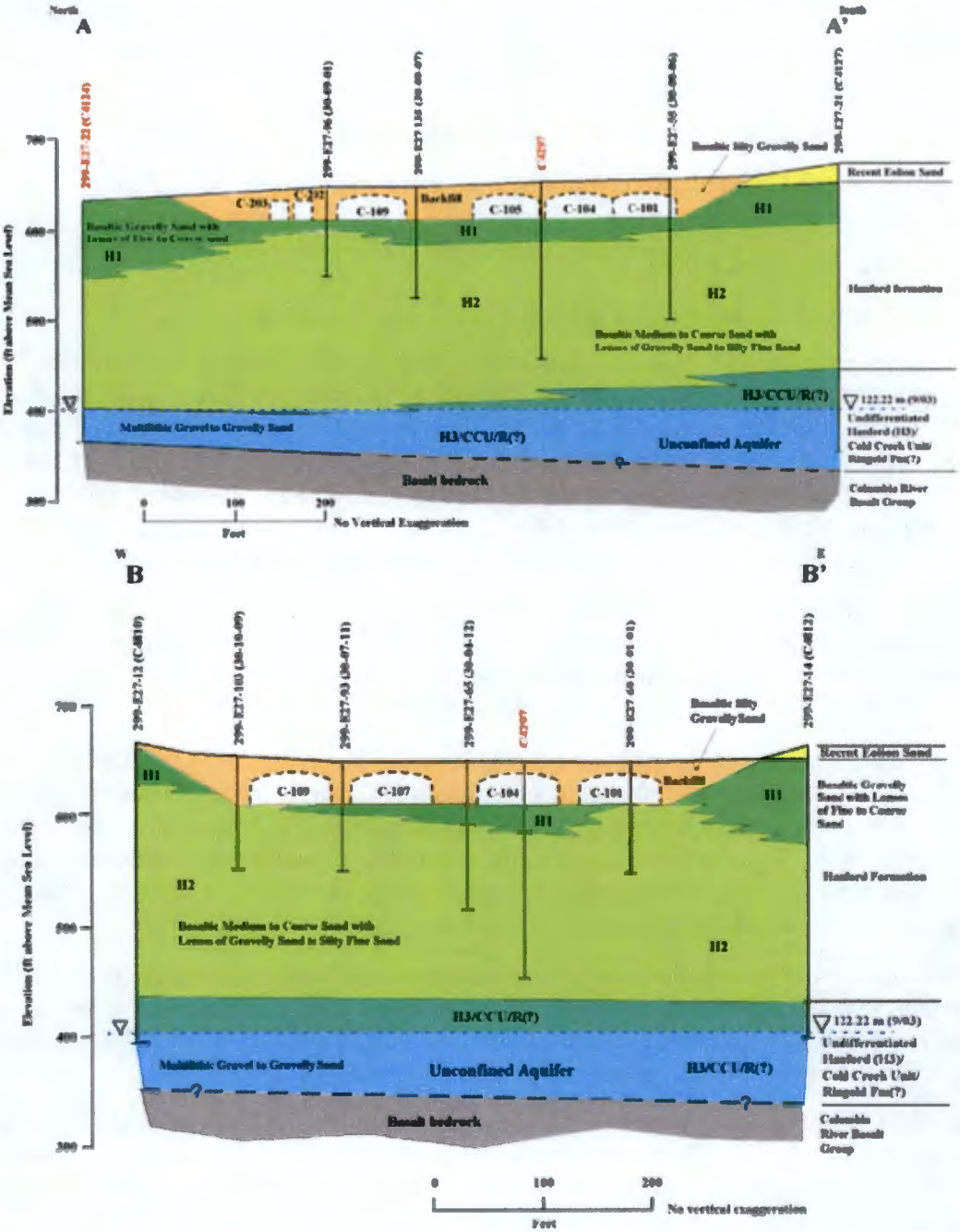

The main source of information regarding geologic strata underlying the Hanford Site and tank farms is data from the drilling of boreholes and analyses of sediments and contaminants within them (e.g., PNNL-14656, *Borehole Data Package for Four CY 2003 RCRA Wells 299-E27-4,*

299-E27-21, 299-E27-22, and 299-E27-23 at Single-Shell Tank, Waste Management Area C, Hanford Site, Washington). More detailed discussion of the borehole-specific geologic and geochemical characteristics of the WMA C vadose zone are provided in RPP-23748, *Geology, Hydrogeology, Geochemistry, and Mineralogy Data Package for the Single-Shell Tank Waste Management Areas at the Hanford Site* and PNNL-15955, *Geology Data Package for the Single-Shell Tank Waste Management Areas at the Hanford Site.*

Three major stratigraphic units underlie C farm, which include in ascending order:

1. The igneous Columbia River Basalt Group and two sedimentary interbed units
2. The undifferentiated H3 unit of the Hanford formation/Cold Creek unit/Ringold Formation (H3/CCU/RF)
3. The Hanford formation (RPP-PLAN-39114).

A general representation of the lateral and vertical distribution of these three units near WMA C along north-south and west-east sections is illustrated in Figure 2-2. The undifferentiated H3/CCU/RF unit directly above the Columbia River Basalt Group is labeled as undifferentiated because two or three major stratigraphic units may have commingled, and clear distinctions between them cannot be made. These include the H3 subunit of the Hanford formation, the Cold Creek unit, and the Ringold Formation's Wooded Island member. Of these, the backfill, Hanford formation, and the undifferentiated H3/CCU/RF make up the vadose zone.

Overall, the vadose zone is 250 to 260 ft thick at WMA C (Figure 2-2). The water table and the associated unconfined aquifer occurs within the H3/CCU/RF units and the overall thickness of this aquifer varies from approximately 55 ft at well 299-E27-155 (south of WMA C) to approximately 38 ft at well 299-E27-22 (north of WMA C).

All major hydrogeologic units are inferred to be essentially continuous in this area, although unit thicknesses vary and some subunits are not continuous. General characteristics of each unit descending from the surface down beneath WMA C are described more fully in Section 2.3.1 of RPP-PLAN-39114. Finally, backfill materials, consisting of poorly sorted cobbles, pebbles, and coarse to medium sand derived from the H1 subunit of the Hanford formation, are distributed around the SSTs and tank infrastructure.

Both water level and general direction of groundwater flow in this region have been altered many times throughout Hanford Site operations history by high-volume wastewater discharges to various ponds (DOE/RL-2008-01, *Hanford Site Groundwater Monitoring for Fiscal Year 2007*; PNNL-16346, *Hanford Site Groundwater Monitoring for Fiscal Year 2006*).

In the 1980s, a groundwater mound in this area was maintained by liquid discharge to B Pond north of WMA C, elevating the water table and imposing a southwestern trend in groundwater flow under WMA C (PNNL-15837, *Data Package for Past and Current Groundwater Flow and Contamination Beneath Single-Shell Tank Waste Management Areas*).

Between 1944 and the mid-1990s, the volume of artificial recharge from Hanford Site operations wastewater disposal was significantly greater than recharge from precipitation. An estimated 1.68×10^{12} L (4.44×10^{11} gal) of liquid was discharged to disposal ponds, trenches, and cribs during this period. Wastewater discharge has decreased since 1984 and currently contributes a volume of recharge in the same range as the estimated natural recharge from precipitation.

Because of the reduction in discharges, groundwater levels are falling, particularly around the operational areas (PNNL-15070, *Hanford Site Groundwater Monitoring for Fiscal Year 2004*).

Current general groundwater flow directions and general flow rates are given in Table 2-1 for WMA C (as adapted from PNNL-15670, *Hanford Site Groundwater Monitoring for Fiscal Year 2005*). The general flow rate has remained unchanged since fiscal year 2005. The water table is very flat over all of the 200 East Area and the most current groundwater flow direction is southwest to south-southwest with a flow rate, based on contaminant migration of sulfate, of 0.09 m per day (DOE/RL-2008-01).

Table 2-1. General Groundwater Flow Directions and Flow Rates for Single-Shell Tank Waste Management Area C in the 200 East Area. (Table 2-2 from RPP-PLAN-39114)

Waste Management Area	Groundwater Flow Direction	Gradient	Groundwater Flow Rate[a,b] (m/day)
C	SW – SSW	0.0001	0.7 to 2.4

Data in table originally reported in PNNL-15670, *Hanford Site Groundwater Monitoring for Fiscal Year 2005*.

[a] Groundwater flow rates are calculated using the Darcy equation.

[b] The multi-stress slug test was used for the calculation of groundwater flow rate for Waste Management Area C.

Reference: RPP-PLAN-39114, 2009, *Phase 2 RCRA Facility Investigation/Corrective Measures Study Work Plan for Waste Management Area C*, Washington River Protection Solutions, LLC, Richland, Washington.

2.3 TANK CONTENTS

The C tank farm received waste generated by essentially all of the major chemical processing operations that occurred at the Hanford Site, including bismuth phosphate fuel processing, uranium recovery, plutonium-uranium extraction (PUREX) fuel processing, fission product recovery and tank farm interim stabilization and isolation activities. Only C tank farm was operational during the bismuth phosphate and uranium recovery processes (RPP-14430).

The C tank farm was constructed between 1943 and 1944 and first received metal waste and first cycle waste from B plant beginning in 1946. Ultimately, SSTs C-101 through C-106 received metal waste and SSTs C-107 through C-112 received first cycle waste. All SSTs were filled with bismuth phosphate waste by the end of 1948. The 200 series SSTs also received metal waste. To free up tank space, in 1952 first cycle waste was transferred to the 242-B evaporator.

Metal waste was also removed from C tank farm beginning in 1952 and transferred to U Plant for uranium recovery. Ancillary equipment involved in the metal waste transfer included the 244-CR vault and diversion boxes 241-CR-151, -152 and –153. Subsequently, tributyl phosphate waste, a byproduct of the uranium recovery process, was returned to C tank farm. The 244-CR vault was modified in 1955 to scavenge tributyl phosphate waste (that is, to separate cesium-137 from the supernatant by precipitation) that was present in SSTs C-107 through C-112. The scavenged slurry was redeposited in SSTs C-109 and C-112 to settle and the resultant supernatant was discharged to the BC cribs, located about 2 miles (3.2 kilometers) south.

The tanks in the C tank farm currently contain an estimated total volume of 1.5 million gallons (5.68×10^6 liters) of mixed wastes consisting of various bismuth phosphate, reduction-oxidation, and PUREX processing waste streams (HNF-EP-0182). General tank content (i.e., liquid and solid volumes) data and some tank monitoring data are summarized monthly in waste tank summary reports (e.g., HNF-EP-0182).

2.4 UNPLANNED RELEASES AT OR NEAR C TANK FARM

There have been a number of unplanned releases reported in and around the C tank farm. A description of these unplanned releases are given in RPP-RPT-42294 *Hanford Waste Management Area C Soil Contamination Inventory Estimates* The largest unplanned releases were associated with transfer of PUREX waste around 1970 and occurred near diversion boxes 241-CR-151, 241-C-151 and 241-C-152 (UPR-81, UPR-82 and UPR-86, respectively). Estimated losses ranged from 2,600 to 36,000 gal (9,800 to 136,000 L). UPR-136 is associated with the SST C-101, which is estimated at approximately 17,000 to 24,000 gal (64,000 to 90,000 L). The remaining eight unplanned releases were primarily small surface spills and airborne contamination.

Although the radiological inventory associated with UPR-81 near the CR-151 diversion box was a reasonably low activity waste stream, it contained approximately 17,000 pounds (7,700 kg) of NO_3/NO_2 combined (RPP-15317, *241-C Waste Management Area Inventory Data Package*).

An overall assessment of the spectral gamma logging data from C farm drywells suggests that most vadose zone contamination in the tank farm originated from surface or near surface sources. This is demonstrated by relatively high concentrations of cesium-137 near surface and a general decrease in cesium-137 activity with depth. Cobalt-60 is found near the bottom of many of the drywells that manifest below near- surface cesium-137 contamination. This indicates that "mobile" cobalt-60 was driven down from subsequent recharge water (rain and snow melt). These contamination events were not generally associated with recorded events and are not comparatively significant sources of vadose zone contamination.

The C tank farm is currently in *Resource Conservation and Recovery Act of 1976* (RCRA) groundwater assessment monitoring. Contaminants present in the groundwater along with potential contamination sources are discussed in PNNL-15670. Figure 2-3 shows the distribution of nitrate from 2005 groundwater data (PNNL-15670) that was collected in the year just prior the period of original data collection. At Hanford, nitrate migrates through the soil practically unimpeded, providing a maximum bound for resistivity imaging. The nitrate concentrations in the vicinity of C tank farm are considerably lower than those measured in tank farm areas previously assessed with SGE (S farm, U farm, and B complex).

Figure 2-3. Nitrate Concentrations (milligrams/liter) Measured in Ground Water Around C Tank Farm – June 2005.

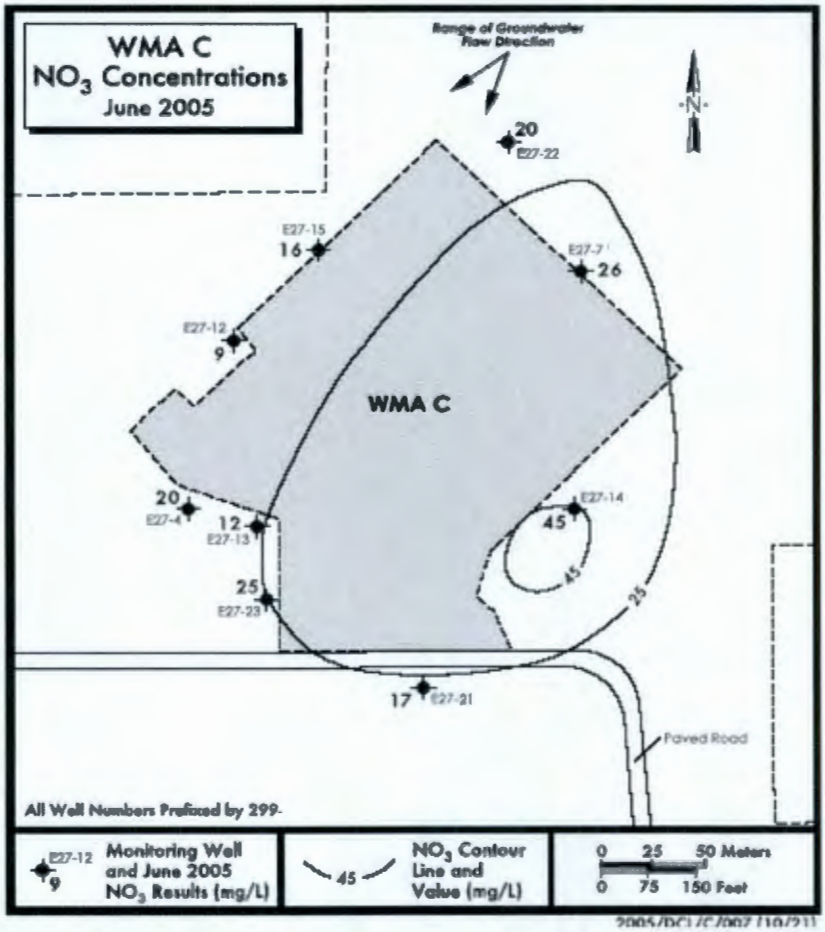

Source: RPP-16608, 2004, *Site-Specific Single-Shell Tank Phase 1 RCRA Facility Investigation/Corrective Measures Study Work Plan Addendum for Waste Management Areas C, A-X, and U*, Revision 1, prepared by J.D. Crumpler, Columbia Energy and Environmental Services, Inc., for CH2M HILL Hanford Group, Inc., Richland, Washington.

2.5 PAST CHARACTERIZATION OF C FARM

A broad range of characterization data and information exists for the C tank farm, including results from geophysical logging of wells and direct pushes (spectral gamma, gross gamma, and neutron), direct soil sampling of vadose zone sediments, and groundwater sampling,. A baseline of geophysical logging occurred on 70 drywells around the tanks in 1997. An update for the geophysical logging is planned for 48 of these wells, as described in the Phase 2 work plan (RPP-PLAN-39114). Specific results from spectral gamma logging in the 1997 study are shown in Figure 2-4. These results show dry well locations where activity levels of cesium-137 greater than 100 pCi/g, greater than 10 pCi/g, and greater than 1 pCi/g were detected. These results also indicate the dry well locations where logging detected cobolt-60 greater than 1 pCi/g. Each of the threshold levels for both cesium-137 and cobalt-60 have a separate symbol. These

measurements suggest that notable areas of contamination can be found near C-101, C-103, C-104, C-105, C-106, and C-109. In a few of the dry well locations, multiple peaks of cesium-137 with depth are indications of the possible occurrence of multiple leak events over time.

Figure 2-4. Results of Spectral Gamma Characterization of Drywells in C Farm, for Cesium-137 and Cobalt-60.

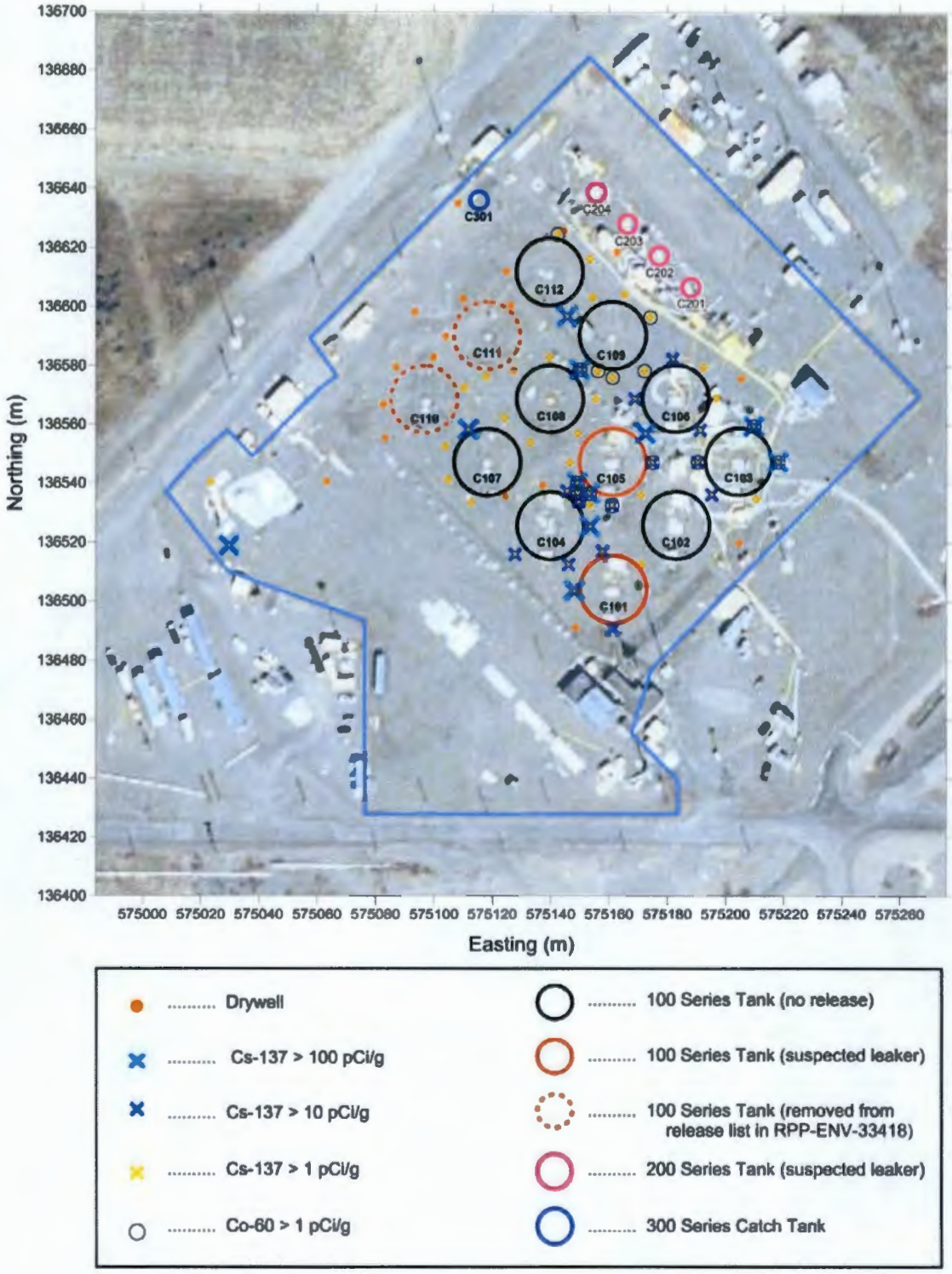

Data from 1997 logging event.

Data that are more comparable to the electrical resistivity characterization are electrical conductivity values measured in porewater extracted from soil cores at characterization borehole locations. Figure 2-5 shows the distribution of borehole locations where samples have been taken. In most cases, pore water samples were extracted and analyzed from only a few soil samples for each borehole. However, borehole C4297 (with 144 samples from 2 to 195 ft below ground surface) located to the northeast of SST C-104 and well 299-E27-22 (with 110 samples from 19 to 230 ft below ground surface) located to the north of the C farm fence line are exceptions. Most of the electrical conductivity (EC) measured in pore water samples show values less than 5 mS/cm (or 2 ohm-m). Results from a few samples, in particular near the UPR-82 release site, show high EC. The highest readings for EC came from pore water extracted from samples from a depth of 42 ft (12.7 mS/cm) at slant direct push location, C5105; from a depth of 61.5 ft (25 mS/cm) in borehole C4297, and from a depth of 28 ft (20.1 mS/cm) in well 299-E27-22. Most direct push borehole locations at UPR-81 did not have accompanying EC data, but had significant nitrate that included a value of 199 μg /g at a depth of 42.5 ft in direct push location, C6394. The maximum nitrate values measured near UPR-86 was 21.4 μg /g at a depth of 18 ft in direct push location , C5960. Similarly, the samples taken near SST C-103 show elevated nitrate values of 90.3 and 192 μg/g at depths of 114 ft and 125 ft in direct push locations, C7466 and C7468, respectively.

Figure 2-5. Electrical Conductivity (EC) Measurements in Porewater Extracted from Soil Samples Taken around C Farm.

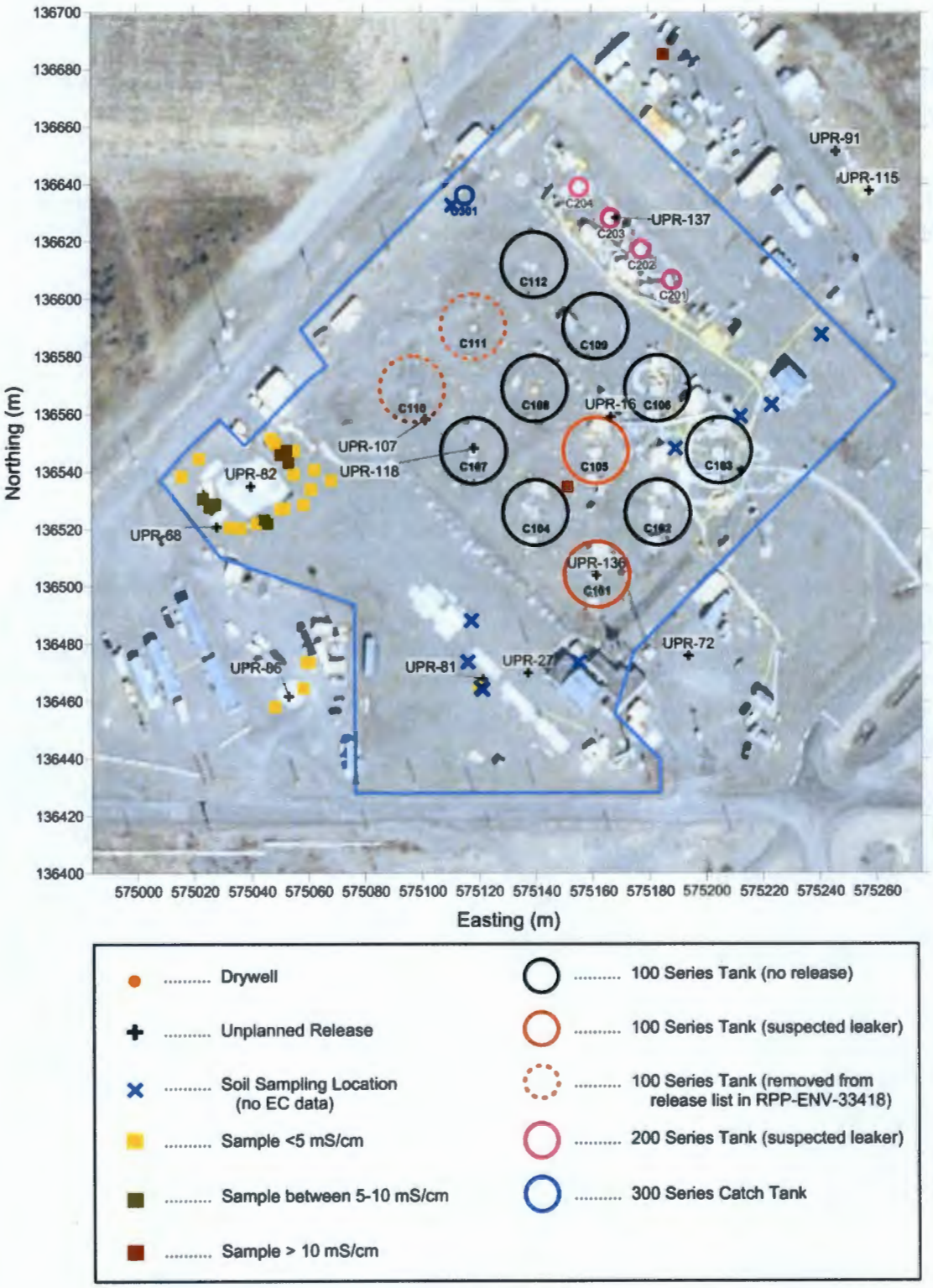

3.0 DATA ACQUISITION—WELL-TO-WELL SURVEY

3.1 SURVEY AREA AND COVERAGE

Remote reference electrodes were installed on August 16, 2006, as the first step in the process of resistivity data collection at the C tank farm complex. Four high resolution resistivity (HRR) survey lines were located parallel to the fence surrounding the tank farm. The HRR lines were offset from the C tank farm perimeter fence at distances of 5 to 131 ft (1.5 to 40 m) as necessary to avoid surface obstacles (Figure 3-1). The surface lines near the tank farm fence line were deployed in an effort to target near-surface characterization activities.

A total of 69 drywells and one buried electrode within the tank farm were used as electrode transmitters and receivers. Additionally, eight groundwater monitoring boreholes outside C tank farm were used as electrode transmitters and receivers. A summary of the data collection phases, methods, and survey coverage area are provided in Table 3-1. Table 3-2 lists the specific wells used in this effort and Figure 3-1 shows the location of the wells used for the SGE survey.

3.1.1 Surface-to-Surface Data Acquisition

Electrodes, embedded into the earth's surface no more than 11 in. (28 cm) in a linear geometrical arrangement, made up a surface electrode array. Each of the electrode stations has the capacity to transmit current or measure voltage. Stainless-steel electrode stakes were permanently installed at 20-ft (6-m) intervals along each array. Approximately 1 L of water or a weak salt solution was introduced at each electrode location to reduce ground contact resistance and improve data quality. Table 3-1 shows that a total of 1.32 line-kilometers of surface resistivity data which were collected during the STS acquisition phase between August 24 and August 26, 2006.

Figure 3-1. Location of Drywells, Groundwater Wells, and Buried Electrodes Used for Surface Geophysical Exploration Survey.

Table 3-1. Summary of Data Coverage.

Survey Phase	Date	Surface HRR			Well and Depth Electrode Tomography		
		Total Coverage	Electrode Spacing	No. Data Points	No. Wells	Well Spacing	Total No. Data Points
STS	East line 8/26/2006	378 m	6 m	1,952	N/A	N/A	N/A
	West line 8/26/2006	234 m	6 m	737			
	North line 8/25/2006	426 m	6 m	2,473			
	South line 8/24/2006	282 m	6 m	1,106			
WTS	East line 8/26/2006	NA	6 m	4,723	77 wells 1 depth electrode	5 – 300 m	17,584
	West line 8/26/2006		6 m	2,917			
	North line 8/25/2006		6 m	5,282			
	South line 8/24/2006		6 m	4,662			
WTW	Forward 8/25/2006	NA	NA	2,799	77 wells 1 depth electrode	5 – 300 m	5,698
	Reverse 8/25/2006			2,899			

HRR = high-resolution resistivity.
m = meter.
NA = not applicable.
STS = surface-to-surface.
WTS = well-to-surface.
WTW = well-to-well.

Table 3-2. Dry Wells and Groundwater Wells Used for Surface Geophysical Exploration Survey. (2 Sheets)

Well ID	SuperSting R8* Channel	Well ID	SuperSting R8* Channel	Well ID	SuperSting R8* Channel
30-00-01	1	30-05-02	27	30-09-02	53
30-00-03	2	30-05-03	28	30-09-06	54
30-00-06	3	30-05-04	29	30-09-07	55
30-00-09	4	30-05-05	30	30-09-10	56
30-00-10	5	30-05-06	31	30-09-11	57
30-00-11	6	30-05-07	32	30-10-01	58
30-05-10	7	30-05-08	33	30-10-02	59
30-00-13	8	30-05-09	34	30-10-09	60
30-00-22	9	Buried Electrode	35	30-10-11	61
30-00-24	10	30-06-02	36	30-11-01	62
30-01-01	11	30-06-03	37	30-11-05	63
30-01-06	12	30-06-04	38	30-11-06	64
30-01-09	13	30-06-09	39	30-11-09	65
30-01-12	14	30-06-10	40	30-11-11	66
30-03-01	15	30-06-12	41	30-12-01	67
30-03-03	16	30-07-01	42	30-12-03	68
30-03-05	17	30-07-02	43	30-12-09	69
30-03-07	18	30-07-05	44	30-12-13	70
30-03-09	19	30-07-07	45	**299-E27-15**	71
30-04-01	20	30-07-08	46	**299-E27-12**	72
30-04-02	21	30-07-10	47	**299-E27-13**	73
30-04-03	22	30-07-11	48	**299-E27-23**	74
30-04-04	23	30-08-02	49	**299-E27-21**	75

Table 3-2. Dry Wells and Groundwater Wells Used for Surface Geophysical Exploration Survey. (2 Sheets)

Well ID	SuperSting R8* Channel	Well ID	SuperSting R8* Channel	Well ID	SuperSting R8* Channel
30-04-05	24	30-08-03	50	**299-E27-14**	76
30-04-08	25	30-08-12	51	**299-E27-7**	77
30-04-12	26	30-09-01	52	**299-E27-22**	78

*SuperSting R8 is a trademark of Advanced Geosciences, Inc.

Groundwater wells are identified in bold. (All other well location reflect dry well locations)

3.1.2 Well-to-Surface and Depth Electrode-to-Surface Data Acquisition

Well-to-surface (WTS) and depth electrode-to-surface data (DTS) acquisition follows the same logic presented in the section above; however, the geometry with respect to drywells, groundwater monitoring wells, buried electrodes, and surface electrodes is distinct from a linear surface array. With WTS and DTS data acquisition, the wells and depth electrode(s) act as the source current, while the surface stations are reserved as receiving electrodes for recording of voltage measurements.

3.1.3 Well-to-Well and Well-to-Depth Electrode Data Acquisition

Well-to-well (WTW)and well-to-depth electrode (WTD) data acquisition follows the same process presented in the above sections. The major difference is the geometry of the electrodes with respect to the wells. The typical electrode used in electrical resistivity is a surface electrode, which is imbedded no more than 11 in. (28 cm) into the ground by design. For all practical purposes, the surface electrode can be represented as a point in model space. A drywell or a groundwater well , however, represents a very long electrode that must be modeled as a line source in the model. Furthermore, drywells or groundwater wells are not generally distributed in a linear fashion. Thus, the end result is a more complex geometrical configuration of sources and receivers which are used to generate a record of observed measured voltage potentials in a fixed sequence of time.

For the WTD survey, a single electrode was installed at a depth of 59 ft (18 m) below the ground surface in order to help provide depth information in the inversions of the WTW measurements. For completeness, reciprocal measurements of WTD and buried electrode-to-well measurements were acquired. For this reanalysis, the single depth electrode was not used in the modeling.

An HRR survey uses a four-electrode array where electric current is injected into the earth through one pair of electrodes (transmitting pole) and the resultant voltage potential is measured by the other pair of electrodes (receiving pole). Reciprocal measurements are recorded where each electrode is used as a receiving and transmitting electrode. In this way, two data sets are generated (forward and reverse) under each geometric array configuration. Figure 3-2 and Figure 3-3 show the forward and reverse measurements for the pole-pole configuration, where for each electrode pair one of the electrodes (electrodes 3 and 4) are effectively at infinity.

Electrical theory shows that reciprocal measurements should be nearly equal, even when acquired under heterogeneous earth conditions. Therefore, comparison of the reciprocal measurements is an effective tool for detecting suspect data, or data influenced by subsurface infrastructure.

Figure 3-2. Forward Pole-Pole Electrode Measurement.

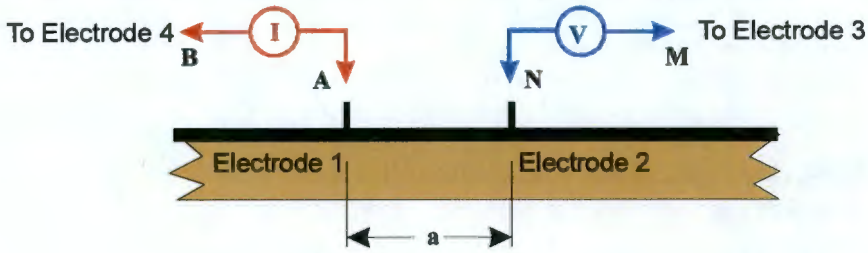

Figure 3-3. Schematic of Reverse Pole-Pole Electrode Measurements.

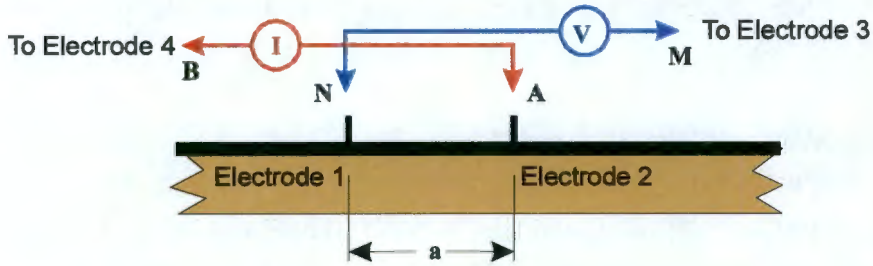

Where:

I = Current electrode pair
V = Voltage electrode pair
B = Remote Reference Current Electrode (placed at infinity)
M = Remote Reference Voltage Electrode (placed at infinity)
N = Local voltage electrode
A = Local current electrode
a = distance between electrodes.

3.2 INSTALLATION AND SETUP

Following the installation of the remote reference electrode arrays, individual 16-gauge wires were strung from a central location outside the C tank farm fence to each of the 69 dry wells and 8 groundwater wells and one depth electrode that would be used as sources and receivers. Wells were prepared in one of two ways: (1) by removing a small area of rust from the well casing and sandwiching a short length of wire between the well casing and the expansion plug used to seal the drywell, or (2) using hose clamps to attach the wire to monitoring components inside the well casing. The wires from the wells were then connected to a patch panel which organizes the

77 wells and one depth electrode wires and acted as a coupler to the SuperSting R8[1] switch boxes. By distributing the measurements in a logically structured method, the switch boxes act as a multiplexer to the SuperSting R8 keeping the data structured. Figure 3-4 is a photograph showing the equipment setup and Figure 3-5 shows the wire-to-well connection.

Figure 3-4. Field Setup and Equipment for the Well-to-Surface Survey.

[1] SuperSting R8 is a trademark of Advanced Geosciences, Inc.

Figure 3-5. Field Worker Attaching Wire to Well.

3.2.1 Installation of Remote Reference Arrays

Remote reference electrode arrays were established approximately 1 mile (1.7 kilometers) from the general area of the survey to the northwest and the northeast of the tank farm site. Each array consisted of 11 stainless steel rods that were driven into the ground and connected together with 10 gauge insulated copper ground wire. A weak salt solution was introduced to each electrode in the source array while water was introduced to each electrode in the receiving array to reduce ground contact resistance and improve data quality. Both remote arrays were connected to the SuperSting R8 using 16-gauge wire. The wire was strung along access roads and through open fields avoiding site infrastructure. The connection of the resistivity equipment to the remote reference electrodes completed the HRR four-pole measurement system. A more detailed description of the installation practice can be viewed in RPP-RPT-28955, *Surface Geophysical Exploration of T Tank Farm*.

3.2.2 Permanent Surface Electrodes

Permanent surface electrodes were installed along four survey lines to streamline the data acquisition activities and improve future data acquisition repeatability. Each electrode consisted of 1/2-in. (1.3 cm) diameter stainless-steel rod in the shape of a "T." The top horizontal bar rested on the ground surface, increasing electrode to ground contact and limiting the electrode penetration to 11 in. (28 cm). Additionally, the top bar also provided a suitable location for connecting the data acquisition cable. The installation of permanent electrodes provides cost reduction as they can be installed without impacting data acquisition time, and once installed can be used many times.

3.2.3 Resistivity Equipment

Electrical measurements were acquired using a SuperSting R8 in a pole-pole array configuration. A combination of passive cables using automated electrode switching boxes, and active cables where the electrode switching is performed on the cable, were used to connect the surface electrodes to the SuperSting R8 data acquisition unit. Two 12-volt direct current marine deep cycle batteries were used to supply input power. The batteries and power cable were strictly controlled using appropriate lockout and tagout procedures. A more comprehensive description of the equipment can be viewed in RPP-RPT-28955.

3.3 RECIPROCAL DATA COLLECTION

Two sets of data were acquired for the WTW dataset: an initial (forward) set and a reverse set. An example raw WTW dataset is shown in Figure 3-6, where transfer resistance is plotted against the distance between the wells conducting voltage measurement and current injection; the figure represents the data acquired in the forward mode. The data also includes all combinations, such as drywell to drywell, drywell to groundwater well, and groundwater well to groundwater well. With each combination the survey resulted in the acquisition of 2,797 data values (Figure 3-6).

Figure 3-6. Scatter of WTW Transfer Resistance Data from WMA C.

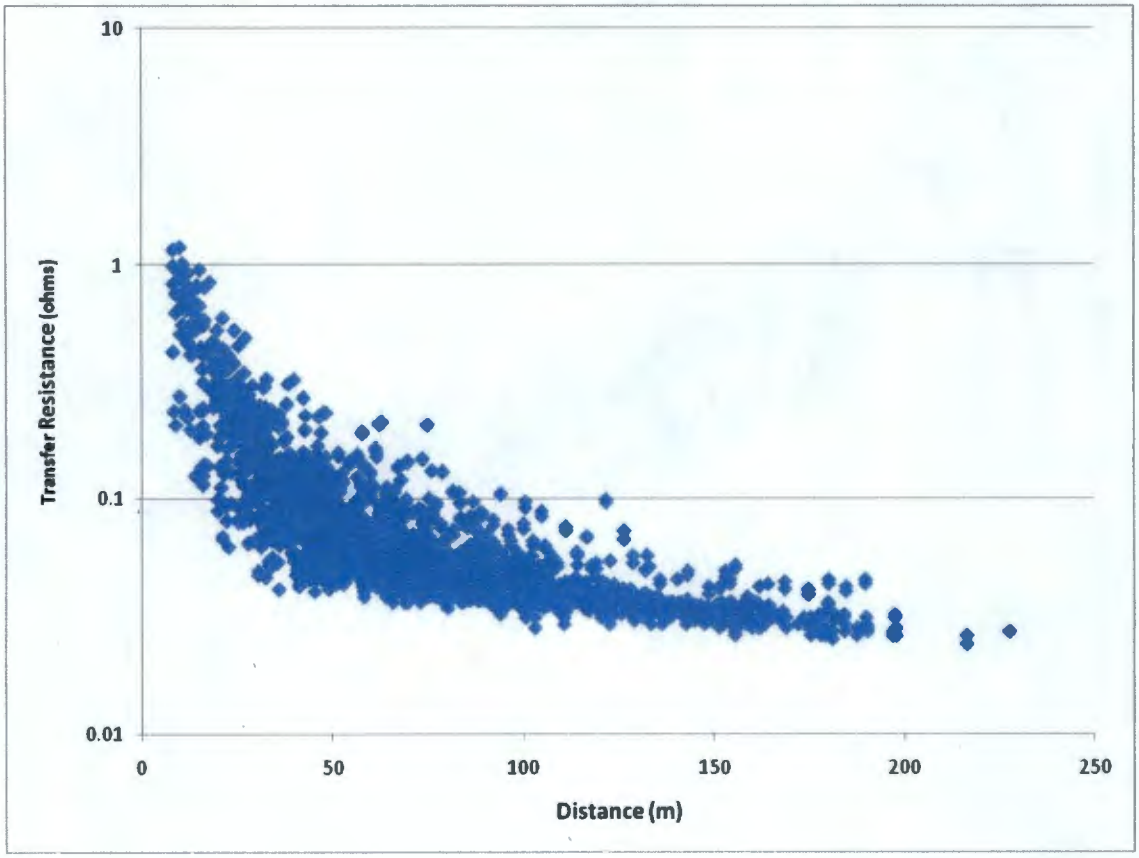

Figure 3-7 shows the scatter of data from the forward dataset for WTS. The forward survey resulted in acquisition of 13,694 measurements. A comparison of the scatter of measurements in the two surveys suggests that the overall distribution of the transfer resistance with distance is slightly higher in the WTW survey than in the WTS survey. This difference in the distribution of transfer resistances between the surveys is not likely due to environmental conditions, and more likely the result of how the wells are used in the voltage measurements relative to the surface electrodes.

Figure 3-8 shows the scatter for the transfer resistance data with distance in the STS survey. A comparison of the results of the STS survey suggests that both the range and the overall distribution of the transfer resistances collected in this survey are greater than that observed from results collected in the WTW or WTS surveys. Given that the resistivity measured with the STS is much more localized near the surface lines compared to data acquired with wells, these apparent differences in transfer resistences likely represent the varied conditions of the periphery of the farm, such as the degree of infrastructure and drier background soils.

Figure 3-7. Scatter of WTS Transfer Resistance Data from WMA C.

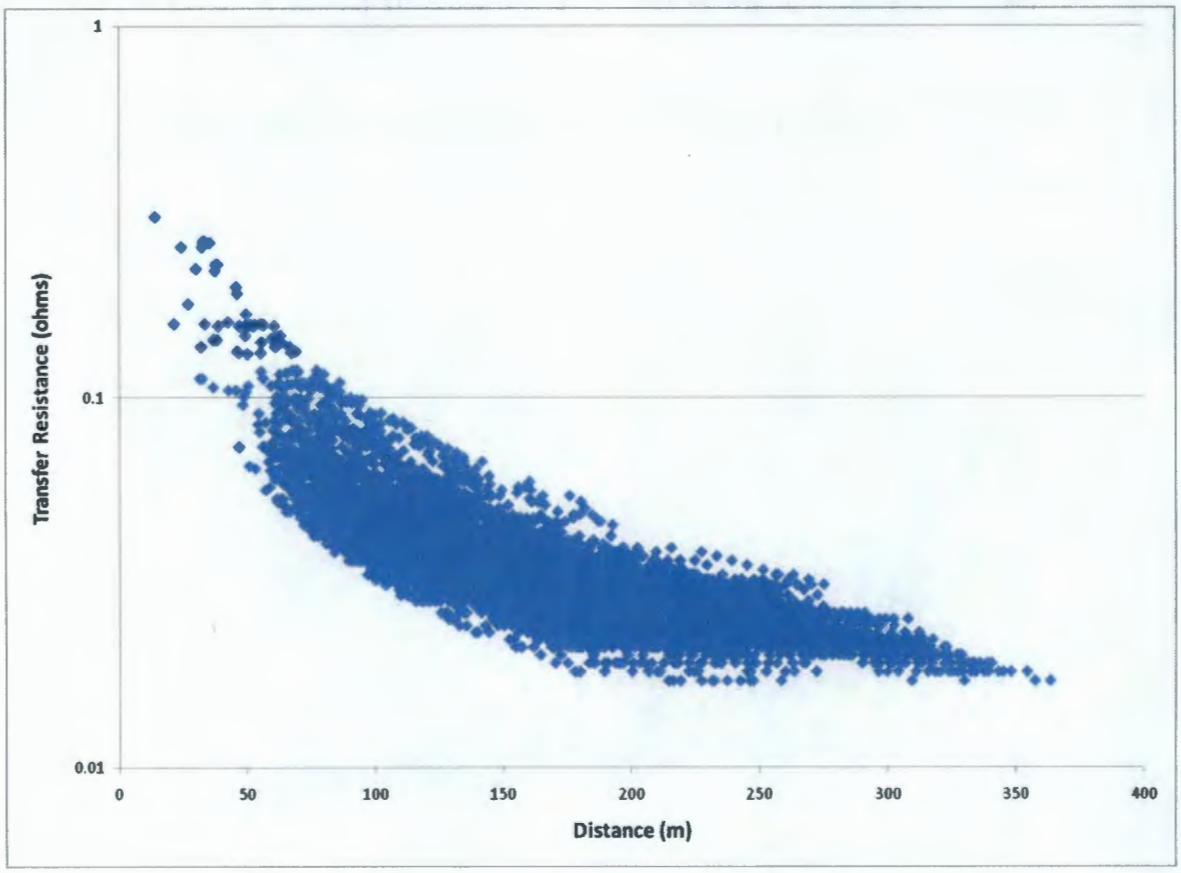

Figure 3-8. Scatter of STS Transfer Resistance Data from WMA C.

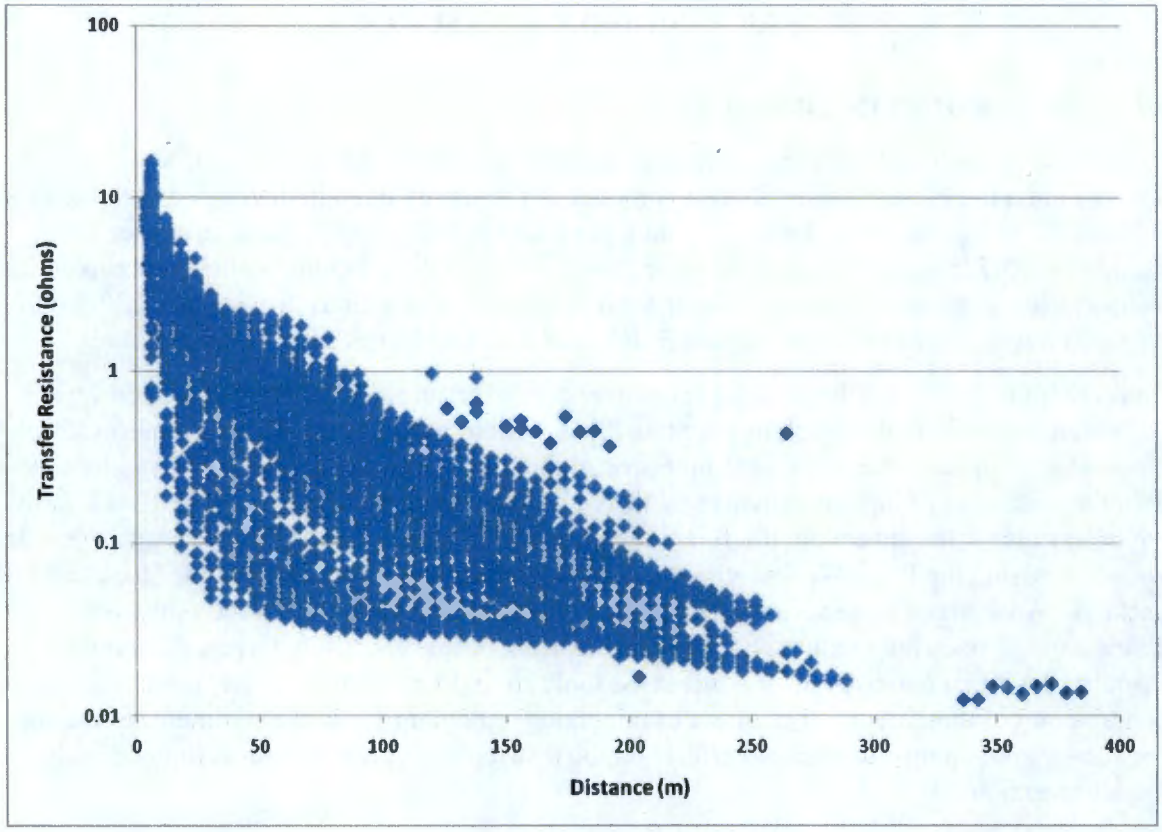

4.0 MODELING RESULTS

4.1 NEW MODELING RESULTS

Upon completion of data filtering, measured apparent resistivity data from the C tank farm site was used in a three-dimensional inversion model of the survey domain developed with the newer RES3DINVx64 software package. Previous modeling efforts for the C tank farm used EarthImager3D (Section 4.2). For specific details of the SGE resistivity method and theoretical basis applied to inverse modeling, the reader is referred to discussions provided in RPP-34690, *Surface Geophysical Exploration of the B, BX, and BY Tank Farms at the Hanford Site.*

To accomplish the three-dimensional (3D) inversion, every surface and long electrode was geo-referenced (using the Washington State Plane – Meters coordinate system) to allow absolute placement of an electrode within the inversion algorithm and model domain. The model was then run with a set of input parameters that have been demonstrated to work well in tank farm environments. After inversion, the final inversion results were interpolated to a regular grid and visualized using the Rock Works™ visualization software package and Surfer® surface contouring package. Analysis of these visualizations facilitate technical evaluation of the estimated distribution of resistivity values and the identification of low resistivity targets that could be associated with increased moisture, increased ionic strength of the pore water, infrastructure, or a combination of these items. The effect of mineralogy and porosity in the sediments evaluated in the survey are assumed to minimal effects on the distribution of resistivities estimated in the model inversion.

The inversion modeling for the C tank farm data considered measurements on 68 wells as long electrodes and 46 surface electrodes. Wells within 6 m of an adjacent well were removed from the domain to minimize the number of very small inversion model cells. The distance-based filtering removed 9 of the 77 wells, leaving 68 for consideration in the inversion models. To further reduce the model complexity, the surface electrodes evaluated in the inversion modeling were decimated to 25 percent of the available electrodes.

To create the final datasets for inversion, two types of data reduction occurred between the data acquisition and final plotting phases. First, data quality was inspected to eliminate unacceptable data that may have resulted from instrumentation error, electrical interference, or high data misfit with respect to neighboring points. The process of removing spurious data points is referred to as editing and is performed prior to the first inversion run. Second, data were filtered after each inverse model was completed to remove data points that contributed to a high model root-mean-square (RMS) error. This process is referred to as a filter run, and the objective of a filter run was to get the final RMS to an acceptable level. Each model was assigned a model number which designated a specific data set or set of modeling parameters and each filter run was assigned a number. An example label for a model with a filter run is "Model_001i."

™ Rock Works is a trademark of Rockware, Inc.
® Surfer is a registered trademark of Golden Software, Inc.

The model used to evaluate the C tank farm dataset focused on the highest quality STS measurements collected along the periphery of the tank farm, the WTS measurements, and the WTW measurements. A high quality dataset for inversion was obtained by removing those data with repeat errors greater than 2 percent and reciprocal errors greater than 5 percent. After noisy data removal, a total of 6,431 data values remained for consideration in the model. After completing the filtering phases to remove additional spurious data, a total of 5,940 data remained for evaluation in the inversion. Table 4-1 lists the statistics for the inversion of the final model, CFarm_006, and Figure 4-1 shows how the data are distributed in a transfer resistance vs. distance plot.

Table 4-1. Inverse Modeling Data File Statistics.

Model	Surface-to-Surface	Well-to-Surface	Well-to-Well	Sum
CFarm_006	177	2998	3256	6431

Figure 4-1. Transfer Resistance Versus Distance Data Used in the Inverse Model.

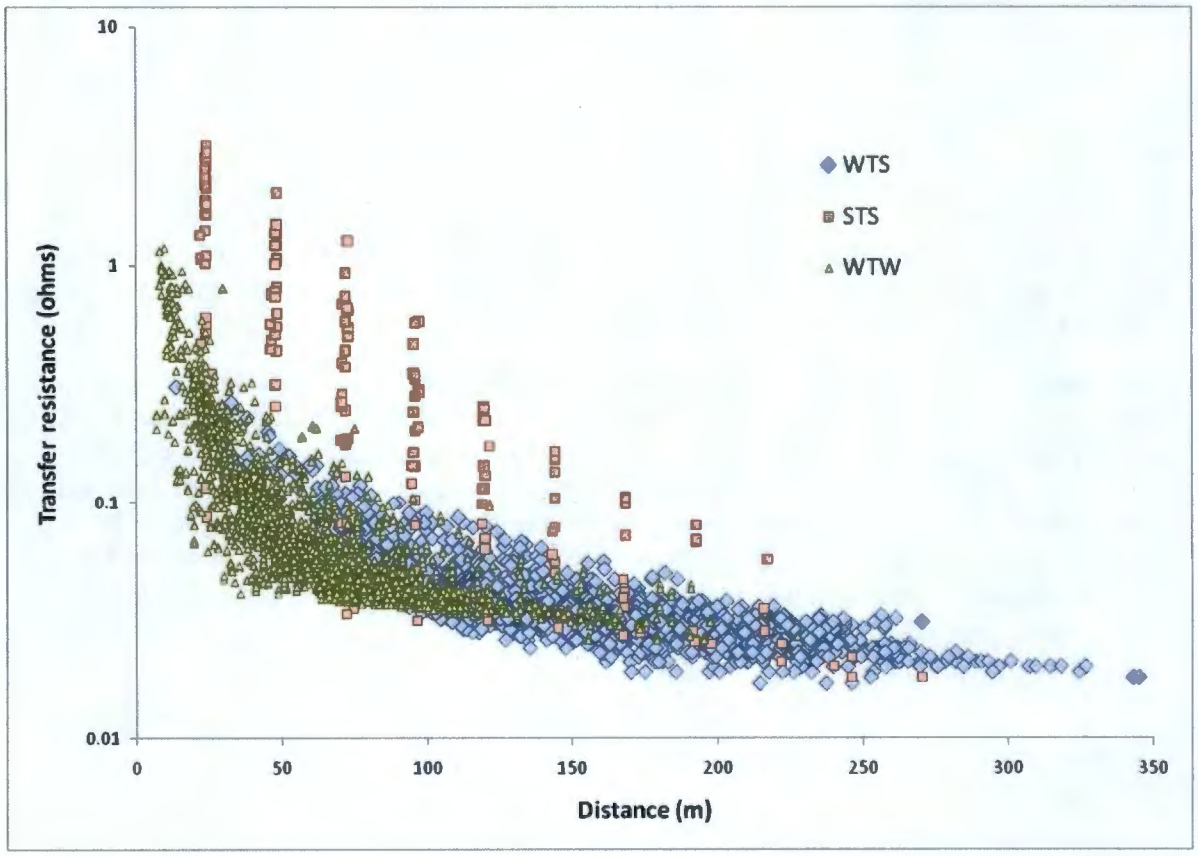

As with any numerical model, a mesh was created whereby the subsurface was discretized into blocks and nodes. The equations that describe the potential field during electrical current

transmission are then solved at every node with the appropriate boundary conditions. RES3DINVx64 automatically generates the mesh for this forward model's calculations by placing grid lines at the intersection of electrodes. Additional requirements of the numerical model include explicitly assigning every block an initial resistivity value and every node a current source (if any).

The final piece of information entered into the inverse model input file was the location of the water table. The water table was entered as *a priori* information due to its known conductive effects. The water table was located at 76 m below ground surface and assigned a resistivity value of 100 ohm-m.

The results of the inverse modeling are shown in Figure 4-2. The figure was constructed from the output file for the fourth iteration of the filtered model run (with a final RMS error of 11.95 percent) and shows a slice of the uppermost model layer. For reference, the location of each well and surface electrode is displayed along with the approximate location of all recorded UPRs.

The estimated distribution of electrical resistivity resulting from the final inversion model, CFarm_006, shows a very low resistivity target centered at SST C-101. Several other smaller targets are identified south of SST C-103, west of SST C-107, in and around SST C-105, and around UPR-82. The quality of each target is affected by the size, intensity (i.e., resistivity contrast relative to background), and number of electrodes near the target. A target of lowest quality would be one in which few electrodes (either wells or surface electrodes) exist nearby, such as the UPR-82 target. A low quality target would warrant further investigation. A high quality target would be one in which several nearby electrodes exist and all effectively confirm the presence of the target, such as that beneath C-101. Intermediate quality targets include south of SSTC-103, where two wells define the lowest resistivity portion of the target, and several more show a feature extending northward beneath the tank to the north side. The target to the west of SST C-107 is of intermediate quality. The results also identify an intermediate quality target beneath SST C-104 as well, but the intensity is low.

A 3D perspective of the lowest resistivity data within the model's domain is provided in Figure 4-3. This figure provides a view towards the northwest from the southeast and shows two isopleths representing 5 and 10 ohm-m for the small opaque and large transparent targets, respectively. The feature beneath SST C-101appears to extend deeply beneath the tank and spread to the southwest in the direction of groundwater flow. All other targets shown in Figure 4-2 are not apparent in Figure 4-3 due to the low resistivity values presented in Figure 4-3. Maximum resistivity values at the targets near SST C-103 and C-107 are approximately 20 ohm-m.

Figure 4-2. Plan View Slice (Uppermost Layer at 0.5 m) of Calculated Resistivity for Model CFarm_006.

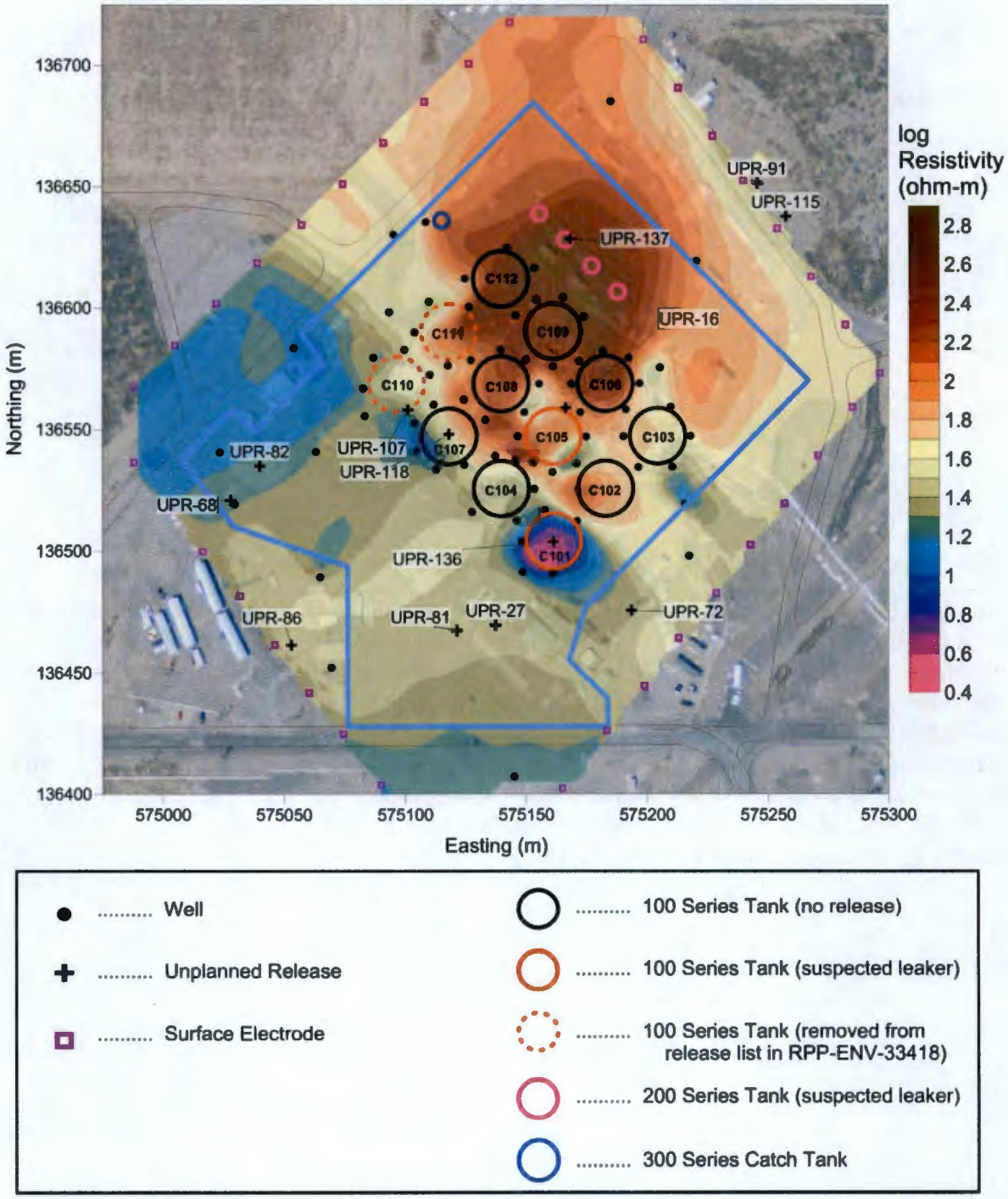

Figure 4-3. Three-dimensional View of a Low Resistivity Target Beneath C Tank Farm, View from Southeast to Northwest for Model CFarm_006.

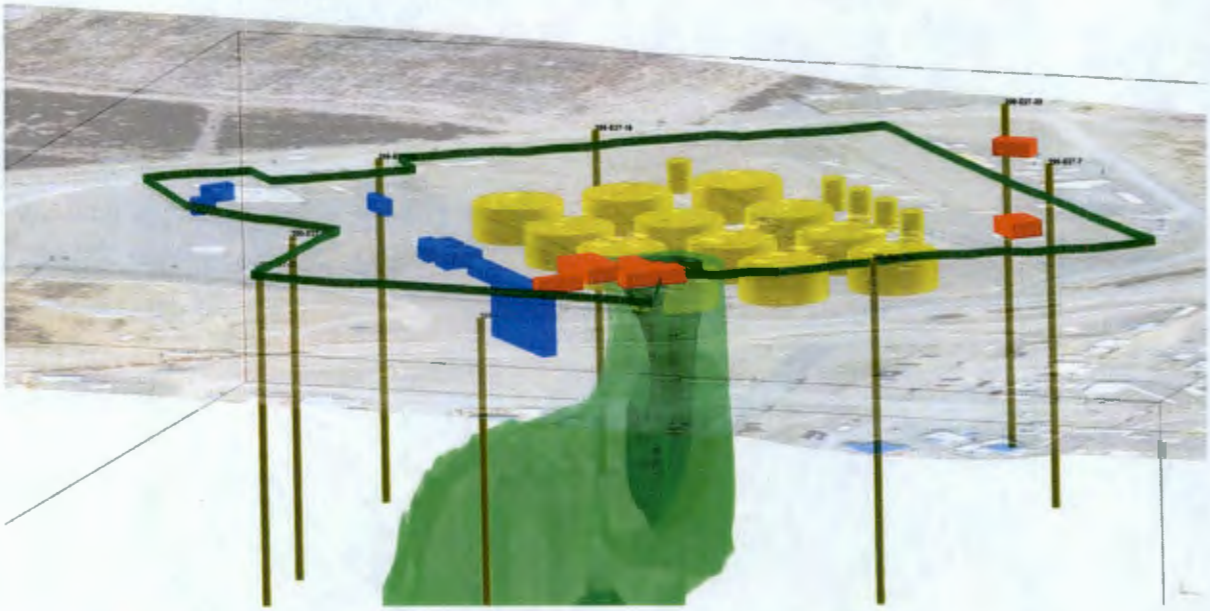

Note: Dark inner opaque plume is 5 ohm-m and lighter transparent outer plume is 10 ohm-m.

Another view of the 3D data, from overhead and from the side looking from the east towards the west is shown in Figure 4-4. The overhead shot shows how the 10 ohm-m contour primarily extends southwest from SST C-101 and C-104 in the direction of the groundwater gradient. A secondary deeper resistivity target can be also seen beneath SST C-108 in the same figure. Interestingly, the SST C-108 target does not appear to have a similar connection to the surface like that of SST C-101 and the origin of the anomaly is unknown. This same resistivity feature also appears to be located below the depth of local dry wells. The original C farm report (RPP-RPT-31558,) reported an anomaly at this location but it is postulated that the low resistivity feature originated from SST C-108.

Figure 4-4. Three-dimensional View of a Low Resistivity Targets Beneath C Tank Farm, Plan View (Top) and View Looking East (Bottom).

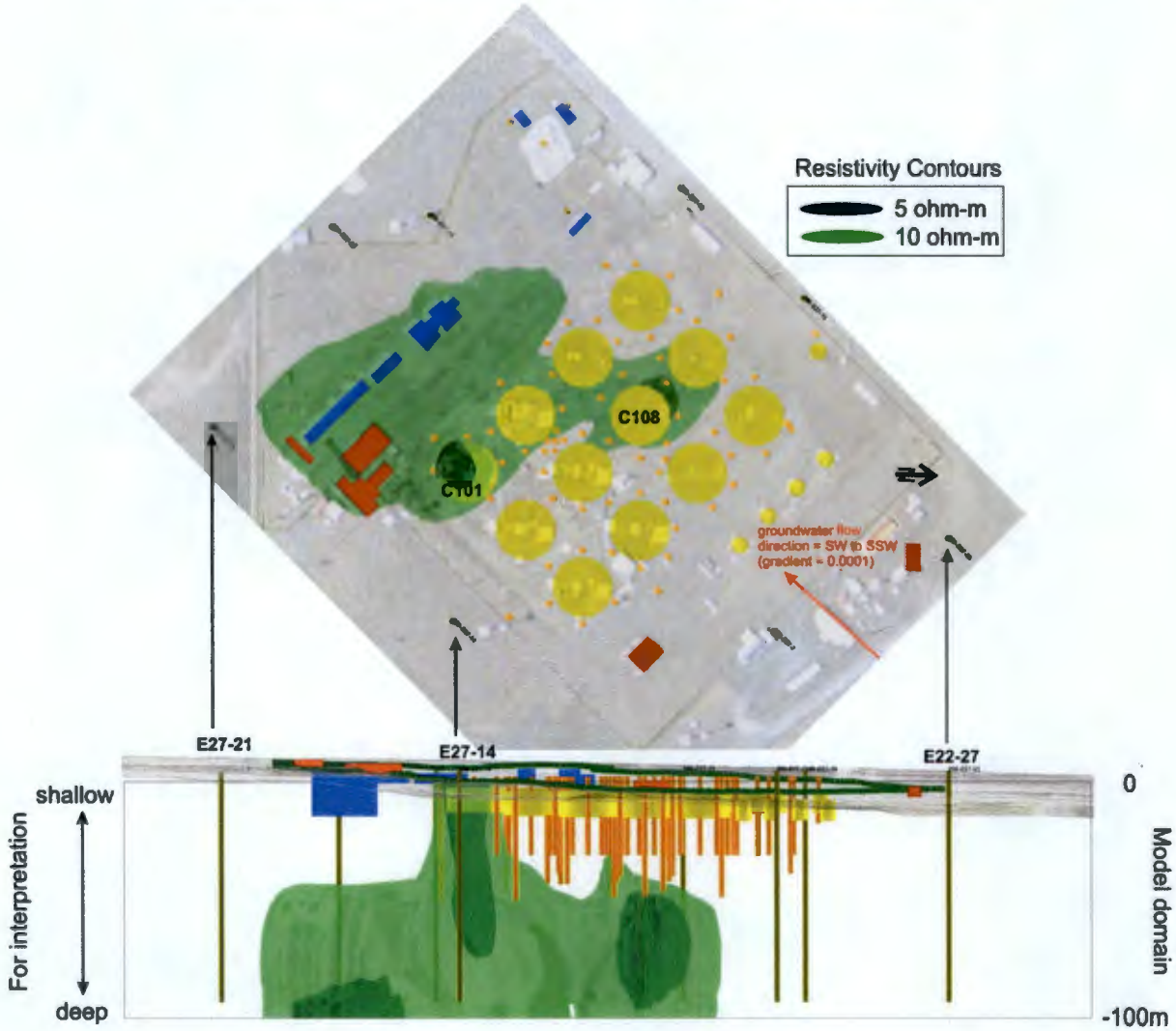

Note: Dark inner opaque plume is 5 ohm-m and lighter transparent outer plume is 10 ohm-m.

Figure 4-5 shows a comparison of the spectral gamma data acquired on the drywells in 1997 (same data presented in Figure 2-4) and the electrical resistivity data. The cesium-137 data are displayed such that if any depth along the well had a value in excess of 1, 10, or 100 pCi/g, a symbol would be displayed for the well. Cobalt-60 data are displayed at only the 1 pCi/g level, because there were no occasions of cobalt exceeding 10 pCi/g. The spectral gamma data are not necessarily indicative of resistivity targets identified in this reanalysis, since the spectral gamma results only show those radionuclides that decay by gamma emission. Electrical resistivity, on the other hand, shows locations of excessive ionic constituents, such as sodium nitrate. This specific figure is provided to show the differences and potentially similarities between this data set and the estimated resistivity distribution. Figure 4-5 shows that most wells had elevated

cesium above 1 pCi/g, with the exception of those wells northwest of SSTs C-110 through C-112. The highest levels of cesium can be found near SSTs C-101, C-104, and C-105. SST C-103, near C-108/109, and C-107/110 also slow a few wells with elevated cesium. The cobalt targets are between SSTs C-104 and C-105, around SSTs C-103, and C-109. The cobalt anomalies for SST C-109 are typically deep, around 80 to 100 ft below ground surface. There does not appear to be a spatial relationship between the low resistivity values of Figure 4-5 and the locations of high levels of cesium or cobalt. Several possible explanations exists that would include:

- Each analyte has a different transport mechanism in the vadose zone
- Cobalt could exist beneath SST C-101 (and coincide with the ionic constituents) but missed by the drywell logging
- Tank waste constituents vary across the farm.

Figure 4-5. Plan View Slice (Uppermost Layer at 0.5 m) of Calculated Resistivity with Spectral Gamma Data Collected in Dry Wells.

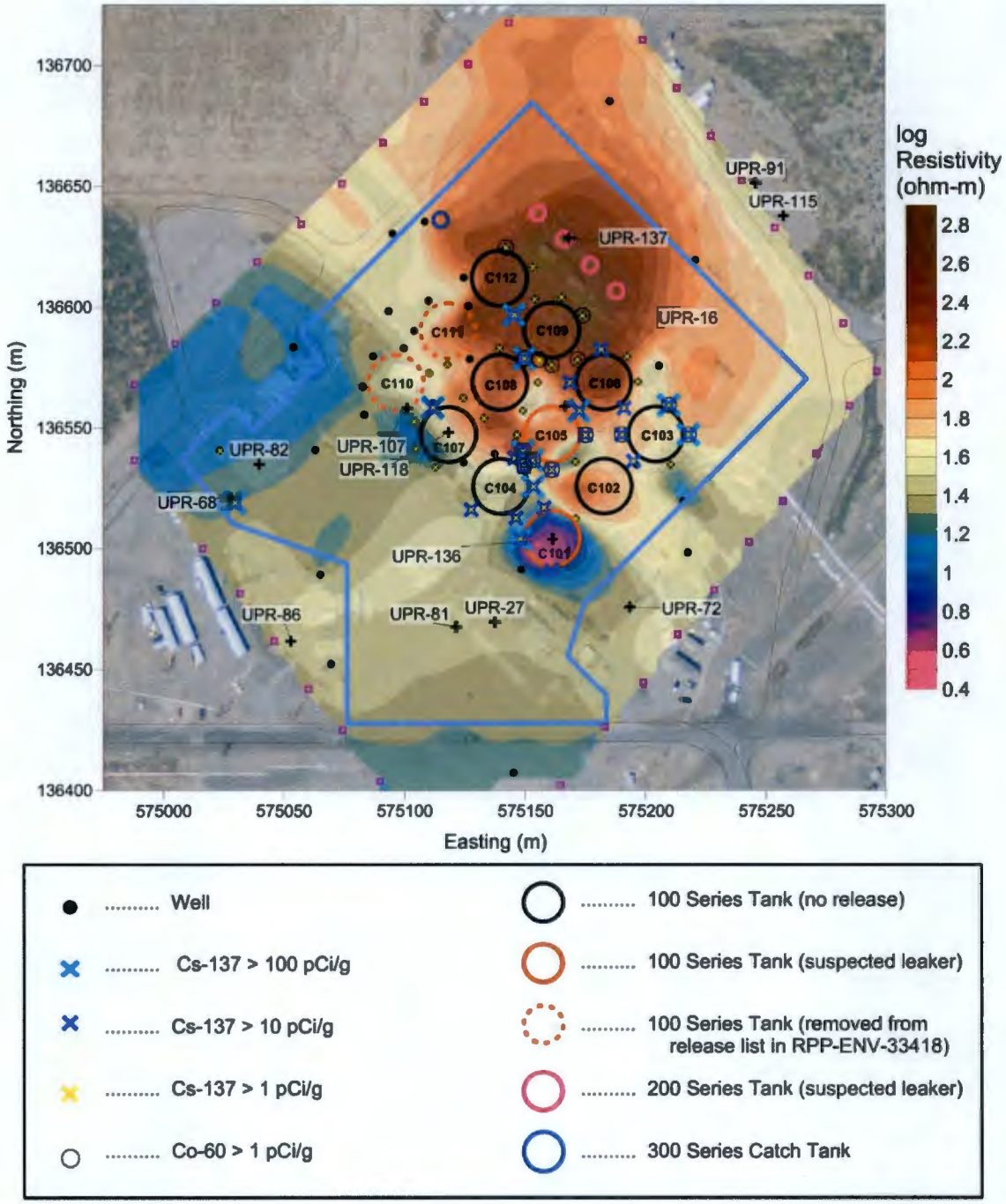

Figure 4-6 shows a comparison between the sampled soil data for electrical conductivity (EC) of the pore water and electrical resistivity estimated for the bulk soil in this reanalysis. There is an expectation of an indirect relationship between pore water conductivity and bulk electrical resistivity, and one would expect to see low resistivity targets near high conductivity porewater

provided that the contaminated porewater is of sufficient size and is relatively shallow for the imaging. However, most of the EC data exists near UPR-82, which is known to be a low resistivity target (albeit of low quality based on electrode distribution). One deep sample taken from a slant borehole was shown to have EC greater than 10 mS/cm (as a reference, samples at BC Cribs were shown to have pore water EC values greater than 150 mS/cm, according to Rucker et al., 2009). The other two locations for electrical conductivity greater than 10 mS/cm are between SSTs C-104 and C-105 and at the groundwater well in the north (E27-22). The northern groundwater well showed one value of elevated pore water conductivity at a depth of 28 ft, and was the likely result of elevated phosphate. Other constituents were relatively low in concentration. The well between the SSTs C-104 and C-105 (C4297) showed a 20-ft zone from 40 to 60 ft, where porewater EC was elevated. Given the intensity of the target beneath SST C-101, soil samples at this location are likely to show a much higher porewater EC than any recorded in the farm to date.

Figure 4-6. Plan View Slice (Uppermost Layer at 0.5 m) of Calculated Resistivity with Electrical Conductivity Data Collected at selected Direct Push Locations.

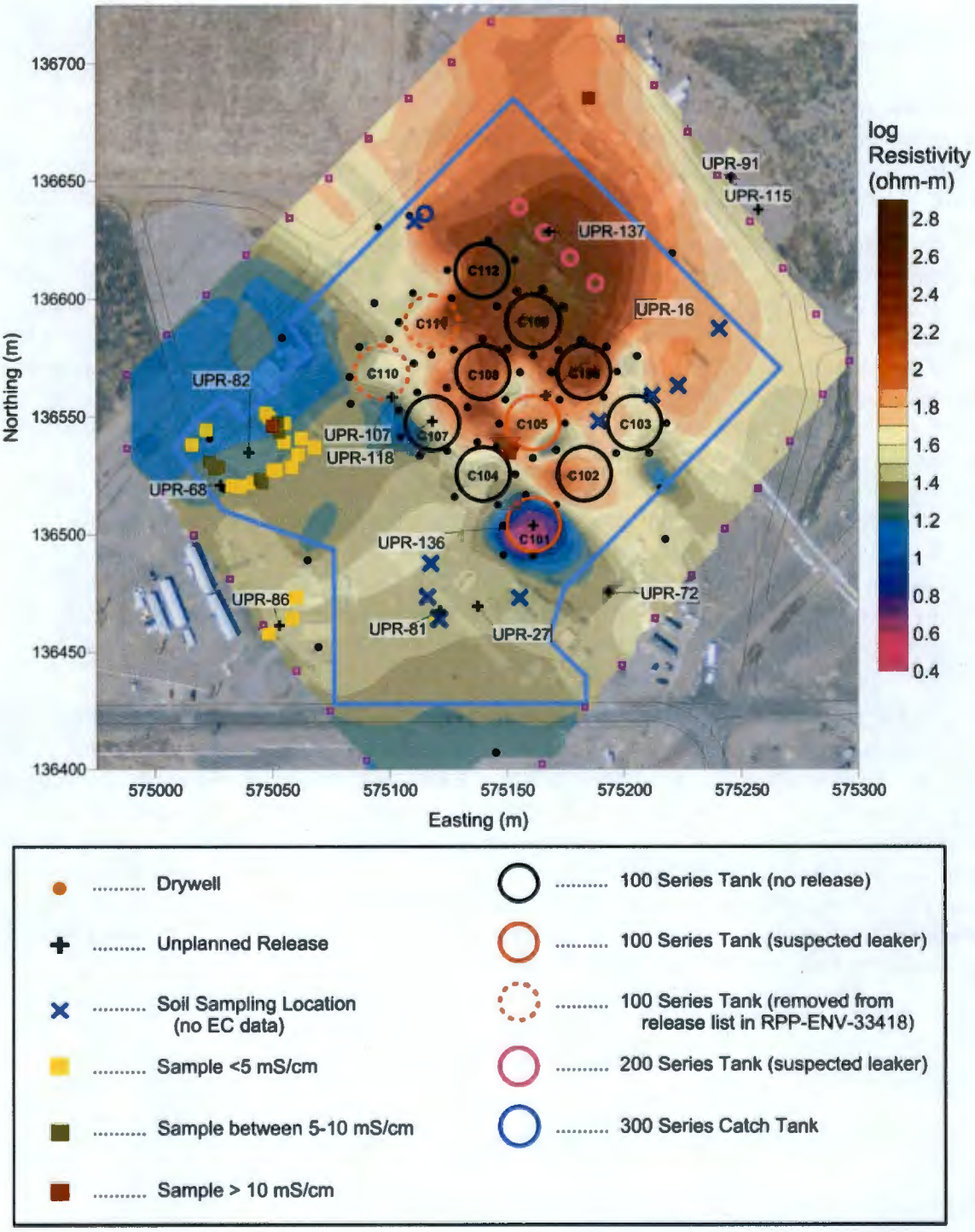

4.2 SUMMARY OF PAST MODELING RESULTS

At the time of the original acquisition of the C tank farm data, the state of the art for processing three-dimensional models included a standard PC with a maximum of 2 GB of RAM and a single processor. Additionally, EarthImager3D was the only commercially-available resistivity inversion software that could accommodate the wells as long electrodes. The processing of the different data types (WTW, WTS, and STS) required splitting the domain into multiple smaller domains and stitching the various mosaics together to produce a final image of the entire C tank farm. To review these limitations, the second paragraph of the 2006 C tank farm report stated:

> "A combination of the size of the tank farm, data collection design, and quality of the surface data provided mixed results from the initial resistivity investigation at the C tank farm. The physical size of the tank farm coupled with the location of the surface lines used for data collection produced more data than could be modeled at one time, given the current computer software and hardware limitations. To perform the resistivity analysis, the model domain had to be broken up into smaller subsets. As a result of the site complexity and modeling limitations, more than 12 different data combinations and model parameters were modeled, which was more than twice that of U farm. Data confidence is greatest where several inversion models are completed using different electrode data sets and/or inversion constraints while still producing similar results. However, despite the increased modeling effort, the individual data subsets produced varying results with a low degree of repeatability. The varying results seem to be caused by the inability to honor the complete data set under this investigation. The well-to-well with the drywell-only data produced the best results in terms of modeling statistics and data confidence..."

For the WTW data alone, 5 different model domains were tested, as shown in Figure 4-7 below. The results of identifying low resistivity targets were mixed, and in general had a low repeatability among the models. The one model mentioned above with the highest confidence (producing the best results) showed a large resistivity target at SST C-104 and SST C-108. Figure 4-8 below shows the results from that model. Rucker et al. (2009) tested the mosaic method of conducting model with smaller cropped domains with Hanford data and also showed low repeatability among the models where low resistivity targets were concerned. The recommendation was to include all of the data that captures a sufficient resistive background to delineate the true edges of the conductive targets.

Figure 4-7. Map of C Farm Showing WTW Inversion Modeling Domains (from RPP-RPT-31588).

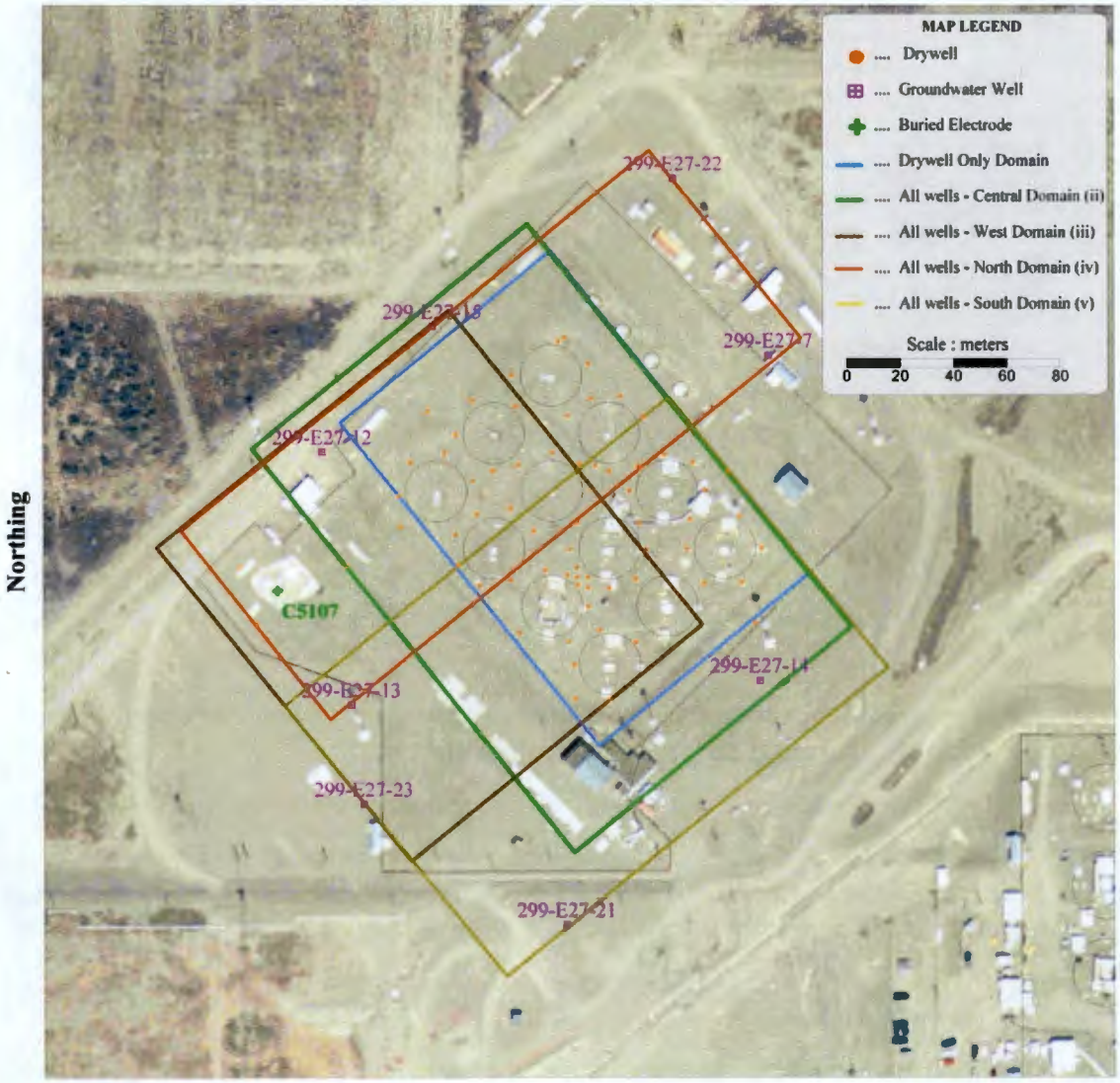

Figure 4-8. WTW Inversion Results using Drywells Only (from RPP-RPT-31588).

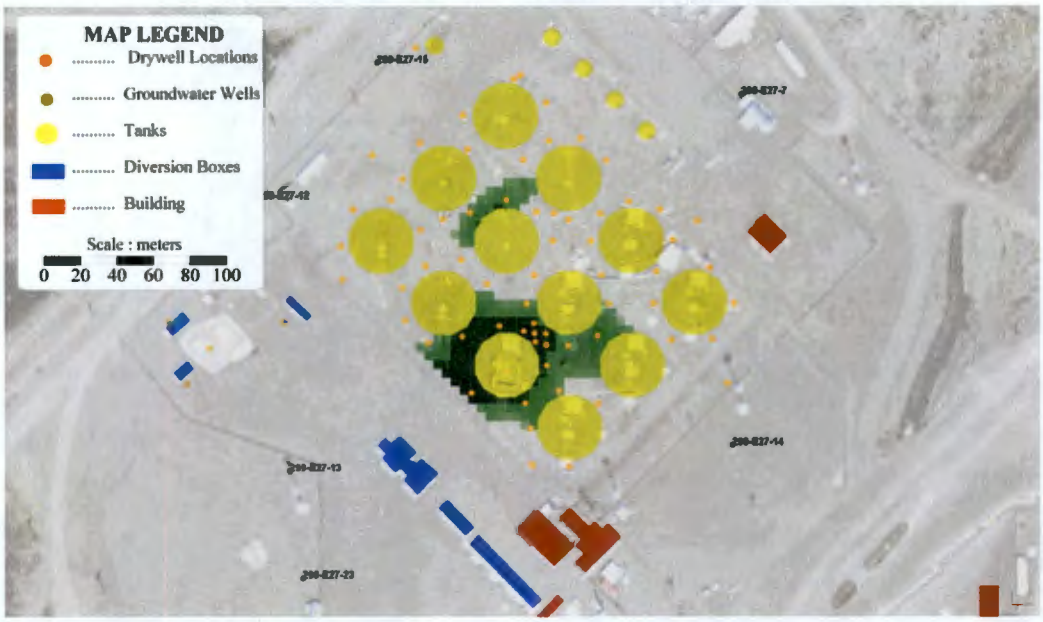

Resistivity Values = 0-4.5 ohm-m Resistivity Values = 0-6.5 ohm-m

In the time since the original C tank farm resistivity acquisition, a number of improvements have been made to acquisition, processing, and interpretation:

- Depth electrode strings installed in direct push holes increases sensitivity of resistivity measurements at depth
- Computer hardware has been increased to accommodate domains that can stretch to over 250 acres
- Inversion software has advanced to more accurately model long electrodes, as shown in Appendix A.

These advancements have significantly enhanced the resolvability of conductive targets with the tank farms. Therefore, given the new capabilities and the limitations highlighted in the original C tank farm report, it is recommended that the results from the original C tank farm report be abandoned for the newer results presented in Figures 4-2 through 4-4 above.

5.0 CONCLUSIONS

An electrical resistivity survey was conducted in the C tank farm to understand the spatial distribution of past waste releases to the vadose zone. The resistivity data were originally acquired in 2006 and processed using existing software tools, which meant dividing the model domain into small overlapping sections in order to be within the 2GB RAM memory limitation of both the computer software and hardware. It has been shown by Rucker et al. (2009) that stitching together multiple overlapping model domains, to form a mosaic comprising electrically conductive targets, will possibly result in a misinterpretation of those targets. To alleviate this issue, it was suggested that all data be processed together in order to form a coherent picture that honors all of the data in a single domain.

The present study reprocessed the C farm data originally acquired in 2006 with newer computer hardware and software that could accommodate all of the data in a single domain. The three dimensional domain was roughly 400 m by 400 m by 100m deep. The survey included the use of wells as long electrodes completed in both the vadose zone and the underlying unconfined aquifer, as well as surface electrodes placed along the periphery of the tank farm. Three resistivity datasets were acquired with all of the electrodes in WTW, WTS, and STS surveys. The data were processed together using the latest version of RES3DINVx64 (v3.03.47). A priori information included explicitly adding information about the water table, including the depth, resistivity value, and confidence in the resistivity value. A relatively low confidence was given to the water table's resistivity of 100 ohm-m (a 2 out of 10, where 10 provides the model with the highest confidence in the water table's properties).

The resulting distribution of resistivity estimated with inversion modeling of the acquired apparent resistivity data showed a significant low resistivity target beneath the SST C-101. Low resistivity is indicative of high ionic strength (or electrical conductivity) porewater or high moisture content. In three dimensions, the target beneath SST C-101 appeared to reach the water table, possibly forming a low resistivity target in groundwater that tends toward the direction of the hydraulic gradient (to the southwest). It has been shown (Rucker et al. 2010) that the vertical resolution from solely using wells as electrodes is extremely poor, as targets tend to appear at the surface layer of the model regardless of the target's depth. However, new modeling using surface electrodes on the periphery of the domain (presented in Appendix B of this report) in combination with wells, shows that targets can be loosely classified as deep or shallow. Based on this, a secondary deep feature appeared beneath C-108, the source of which is unknown. The target associated with SST C-108 also appears disconnected from the surface making it likely that the source could have been from another location and was simply transported to its present location.

Several other low resistivity features appeared in the surface layer of the model that should be investigated further. Most prominently is the target that is near UPR-82, which is presently being investigated as part of another SGE project. Results of the UPR-82 model should be completed by September 2011. Other targets are also seen at SST C-105, SST C-107, beneath SST C-104, and south of SST C-103.

6.0 REFERENCES

ARH-LD-132, 1976, *Geology of the 241-C Tank Farm*, Atlantic Richfield Hanford Company, Richland, Washington.

DOE/ORP-2003-11, 2003, *Preliminary Performance Assessment for Waste Management Area C at the Hanford Site, Washington*, Revision 0, CH2M HILL Hanford Group, Inc., Richland, Washington.

DOE/RL-2008-01, 2008, *Hanford Site Groundwater Monitoring for Fiscal Year 2007*, Revision 0, U.S. Department of Energy, Richland Operations Office, Richland, Washington.

Ecology, EPA, and DOE, 1989, *Hanford Federal Facility Agreement and Consent Order*, as amended, Washington State Department of Ecology, U.S. Environmental Protection Agency, and U.S. Department of Energy, Olympia, Washington.

HNF-EP-0182, 2011, *Waste Tank Summary Report for Month Ending February 28, 2011*, Revision 275, Washington River Protection Solutions, LLC, Richland, Washington.

HW-61780, 1959, *Subsurface Geology of the Hanford Separations Areas*, General Electric Company, Richland, Washington.

PNNL-14656, 2004, *Borehole Data Package for Four CY 2003 RCRA Wells 299-E27-4, 299-E27-21, 299-E27-22, and 299-E27-23 at Single-Shell Tank, Waste Management Area C, Hanford Site, Washington*, Pacific Northwest National Laboratory, Richland, Washington.

PNNL-15070, 2005, *Hanford Site Groundwater Monitoring for Fiscal Year 2004*, Pacific Northwest National Laboratory, Richland, Washington.

PNNL-15670, 2006, *Hanford Site Groundwater Monitoring for Fiscal Year 2005*, Pacific Northwest National Laboratory, Richland, Washington.

PNNL-15837, 2007, *Data Package for Past and Current Groundwater Flow and Contamination Beneath Single-Shell Tank Waste Management Areas*, Pacific Northwest National Laboratory, Richland, Washington.

PNNL-15955, 2007, *Geology Data Package for the Single-Shell Tank Waste Management Areas at the Hanford Site,* Pacific Northwest National Laboratory, Richland, Washington.

PNNL-16346, 2007, *Hanford Site Groundwater Monitoring for Fiscal Year 2006*, Pacific Northwest National Laboratory, Richland, Washington.

Resource Conservation and Recovery Act of 1976, Public Law 94-580, 42 U.S.C. 6901, et seq.

RPP-14430, 2003, *Subsurface Conditions Description of the C and A-AX Waste Management Area*, Revision 0, CH2M HILL Hanford Group, Inc., Richland, Washington.

RPP-15317, 2003, *241-C Waste Management Area Inventory Data Package*, Revision 0, CH2M HIL Hanford Group, Inc., Richland, Washington.

RPP-16608, 2004, *Site-Specific Single-Shell Tank Phase 1 RCRA Facility Investigation/Corrective Measures Study Work Plan Addendum for Waste Management Areas C, A-X, and U,* Revision 1, prepared by J.D. Crumpler, Columbia Energy and Environmental Services, Inc., for CH2M HILL Hanford Group, Inc., Richland, Washington.

RPP-23748, 2006, *Geology, Hydrogeology, Geochemistry, and Mineralogy Data Package for the Single-Shell Tank Waste Management Areas at the Hanford Site,* Revision 0, CH2M HILL Hanford Group, Inc., Richland, Washington.

RPP-34690, 2007, *Surface Geophysical Exploration of the B, BX, and BY Tank Farms at the Hanford Site*, Revision 0, CH2M HILL Hanford Group, Inc., Richland, Washington.

RPP-35484, 2007, *Field Investigation Report for Waste Management Areas C and A-AX*, Revision 1, CH2M HILL Hanford Group, Inc., Richland, Washington.

RPP-PLAN-39114, 2009, *Phase 2 RCRA Facility Investigation/Corrective Measures Study Work Plan for Waste Management Area C*, Washington River Protection Solutions, LLC, Richland, Washington.

RPP-RPT-28955, 2006, *Surface Geophysical Exploration of T Tank Farm*, Prepared by hydroGEOPHYSICS and Columbia Energy and Environmental Services, Inc. for the U.S. Department of Energy, Richland, Washington.

RPP-RPT-31558, 2006, *Surface Geophysical Exploration of C Tank Farm*, Revision 0, CH2M HILL Hanford Group, Inc., Richland, Washington.

Rucker, D.F., M.T. Levitt, and W.J. Greenwood, 2009, "Three-dimensional Electrical Resistivity Model of a Nuclear Waste Disposal Site," Journal *of Applied Geophysics,* 69:150-164.

Rucker, D. F., M. Loke, G. Noonan, and M. Levitt, 2010, "Electrical Resistivity Characterization of an Industrial Site using Long Electrodes," *Geophysics*, Volume 75 (4): WA95-WA104

APPENDIX A

QUALITY ASSURANCE

Collection and analysis of Surface Geophysical Exploration (SGE) data are performed under a project-specific quality assurance plan using a graded approach that conforms to applicable requirements from Columbia Energy and Environmental Services, Inc. (Columbia Energy) quality assurance procedures (CEES-0333, *Quality Assurance Plan for Surface Geophysical Exploration Projects*). These procedures implement the requirements of ASME NQA-1, *Quality Assurance Requirements for Nuclear Facility Applications* and DOE O 414.1C, *Quality Assurance*. Work not covered in the quality assurance plan will conform to accepted industry standards for SGE and sound engineering principles.

This quality assurance plan implements the criteria of DOE O 414.1C and the following requirements from ASME NQA-1:

- Organization (Requirement 1)
- Quality Assurance Program (Requirement 2)
- Instructions, Procedures, and Drawings (Requirement 5)
- Document Control (Requirement 6)
- Corrective Action (Requirement 16)
- Quality Assurance Records (Requirement 17).

Columbia Energy and hydroGEOPHYSICS, Inc. collect data using designed systems or off-the-shelf commercially available hardware. Designed systems conform to applicable requirements in approved procedures that address design, design analysis, design verification, and engineering drawing.

A project specific software management plan, CEES-0338, *Software Management Plan for Surface Geophysical Exploration Projects*, was prepared to implement a graded approach to software management in accordance with the following requirements documents:

- ASME NQA-1, Subpart 2.7, "Quality Assurance Requirements for Computer Software for Nuclear Facility Applications"
- CEES-0333
- CE-ES-3.5, *Software Engineering*
- Contract 28090, *High Resolution Resistivity Characterization of Single Shell Tank Farm Waste Management Areas*
- DOE O 414.1C.

A1.0 DATA PROCESSING

The process used to filter the raw data is described in the system design description (CEES-0360, *Surface Geophysical Exploration System Design Description*). Data are downloaded from the resistivity instrument and parsed into a usable format. Data filtering techniques are then used to remove data spikes or anomalous data caused by data acquisition card instabilities, or extraneous current sources.

Data filtering is performed by copying the parsed raw data into an Excel® data filtering template that contains a series of graphs that show the various data parameters. The process of filtering eliminates data points, but no data modification (rounding, averaging, smoothing, or splining) is permitted. The rationale is to seek out and remove spurious points that do not conform to the data population or points that violate potential theory.

The final step is to inverse model the measured data to obtain the spatio-temporal distribution of electrical resistivity. Inverse modeling is accomplished using either EarthImager3DCL (EI3DCL) or RES3DINVx64 (RES3D). Verification and testing of the inversion software was performed and documented in RPP-34974, *Verification and Testing of the EarthImager Series of Electrical Resistivity Inversion Codes – A Benchmark Comparison*. Verification and testing was performed on the existing two-dimensional (2D) and three-dimensional (3D) versions of the software as well as the upgraded 64-bit, multi-threaded versions developed for tank farm projects.

The objective of the verification and testing study was to demonstrate that the resistivity inversion codes were comparable to known conditions from a pilot-scale field resistivity experiment. The pilot-scale field experiment was used to test the well-to-well (WTW) inversion methodology by establishing a known conductive target in the subsurface and making measurements with a set of 27 simulated wells. To date, there is no industry standard for the WTW resistivity imaging technique, which necessitated the field experiment. The field experiment was designed to test both inversion code's ability to replicate a target of known geometry. The subsurface geophysical target was an amended, electrically conductive soil, buried approximately 1.6 ft (0.5 m) below ground surface. The 27 wells were distributed around the target in a pattern similar to tank B-105 in the B tank farm.

From the above descriptions, it is obvious that data processing is performed using a number of software packages. The requirements and responsibilities for the identification, evaluation, development, testing, and maintenance of quality-affecting software acquired, developed, or modified in support of the SGE efforts are defined in the CEES-0338.

A2.0 REFERENCES

ASME NQA-1, 2004, *Quality Assurance Requirements for Nuclear Facility Applications*, American Society of Mechanical Engineers, New York, New York.

CE-ES-3.5, *Software Engineering*, as revised, Columbia Energy and Environmental Services, Inc., Richland, Washington.

CEES-0333, 2006, *Quality Assurance Plan for Surface Geophysical Exploration Projects*, as revised, Columbia Energy and Environmental Services Inc., Richland, Washington.

CEES-0338, 2006, *Software Management Plan for Surface Geophysical Exploration Projects*, as revised, Columbia Energy and Environmental Services Inc., Richland, Washington.

® Excel is a registered trademark of the Microsoft Corporation.

CEES-0360, 2007, *Surface Geophysical Exploration System Design Description*, as revised, Columbia Energy and Environmental Services, Inc., Richland, Washington

Contract 28090, Requisition 123974, *High Resolution Resistivity Characterization of Single Shell Tank Farm Waste Management Areas*, Revision 3, CH2M HILL Hanford Group, Inc.

DOE O 414.1C, *Quality Assurance*, U.S. Department of Energy, Washington, D.C. Available at: http://www.directives.doe.gov/pdfs/doe/doetext/neword/414/o4141c.pdf.

RPP-RPT-35104, 2007, *Verification and Testing of the EarthImager Series of Electrical Resistivity Inversion Codes – A Benchmark Comparison*, Revision 0, CH2M HILL Hanford Group, Inc., Richland, Washington.

APPENDIX B

THEORY

This chapter provides summary level descriptions for the resistivity inversion modeling. To read a summary of the theory behind the various resistivity techniques, refer to RPP-RPT-28955, *Surface Geophysical Exploration of T Tank Farm.*

B1.0 RESISTIVITY INVERSION PRINCIPLES

The modern application of the electrical resistivity characterization (ERC) method uses numerical modeling and inversion theory to estimate the electrical resistivity distribution of the subsurface from the acquired dataset. The inverse modeling is necessary, as measuring the resistivity is not a direct process. The acquired dataset only contains positions of the electrodes and the measured potential normalized to the injected current. However, the potential values are a result of the spatial resistivity distribution, allowing them to be used indirectly to back-calculate, using an inversion algorithm, an estimate of the true resistivity that gives rise to those potential measurements.

A common resistivity inverse method incorporated in commercial codes is the regularized least squares optimization method. Refer to Sasaki (1989), "Two-dimensional joint inversion of magnetotelluric and dipole-dipole resistivity data," as well as, Loke et al. (2003), "A comparison of smooth and blocky inversion methods in 2D electrical imaging surveys." The objective function aims to minimize the difference between measured and modeled potentials or apparent resistivities (subject to certain constraints) and the optimization is conducted iteratively due to the nonlinear nature of the model that describes the potential distribution. The relationship between the subsurface conductivity σ and the measured potential ϕ is given by equation (1) which is from Dey and Morrison (1979), "Resistivity modeling for arbitrarily shaped three-dimensional structures":

$$-\nabla\cdot\left[\sigma(x,y,z)\nabla\phi(x,y,z)\right]=\left(\frac{I}{U}\right)\delta(x-x_s)\delta(y-y_s)\delta(z-z_s) \qquad (1)$$

Where:

I is the current applied over an elemental volume U specified at a point (x_s, y_s, z_s) by the Dirac delta function. Common methods of solving Equation (1) include:

- The finite difference method (Dey and Morrison 1979)
- The finite element method (Sasaki 1989, as mentioned earlier, and Greenhalgh et al. 2009, "Explicit expressions for the Fréchet derivatives in 3D anisotropic resistivity inversion")
- The analytical element method (Furman et al. 2002, "Electrical potential distributions in response to applied current in a heterogeneous subsurface, solution for circular inclusions")
- The finite volume approach (Pidlisecky et al. 2007, "RESINVM3D: A 3D resistivity inversion package").

The finite-difference method was used in this research.

Regardless of the numerical method, a mesh is created whereby the subsurface is discretized into blocks and nodes. Equation (1) is solved for ϕ at every node with the appropriate boundary conditions. Additional requirements of the numerical model include explicitly assigning every block a resistivity value and every node a current source (if any). Figure B-1a shows a typical mesh for a three-dimensional volume that has been discretized into rectangular blocks over several layers. Figure B-1b shows a more detailed overhead view of the relationship between the mesh lines (in the x- and y-directions), model blocks, and nodes. The potentials are calculated at the nodes that are located at the intersections of the mesh lines, but the resistivity is assigned for the block bound by the mesh lines. Numerical methods work such that finer (or smaller) mesh sizes with more nodes give rise to more accurate solutions, with the trade-off of solution efficiency and computer memory requirements.

Figure B-1. a) Discretized Earth for Inversion, b) Overhead View of Meshing Showing Relationship Between Nodes, Mesh Lines, and Blocks.

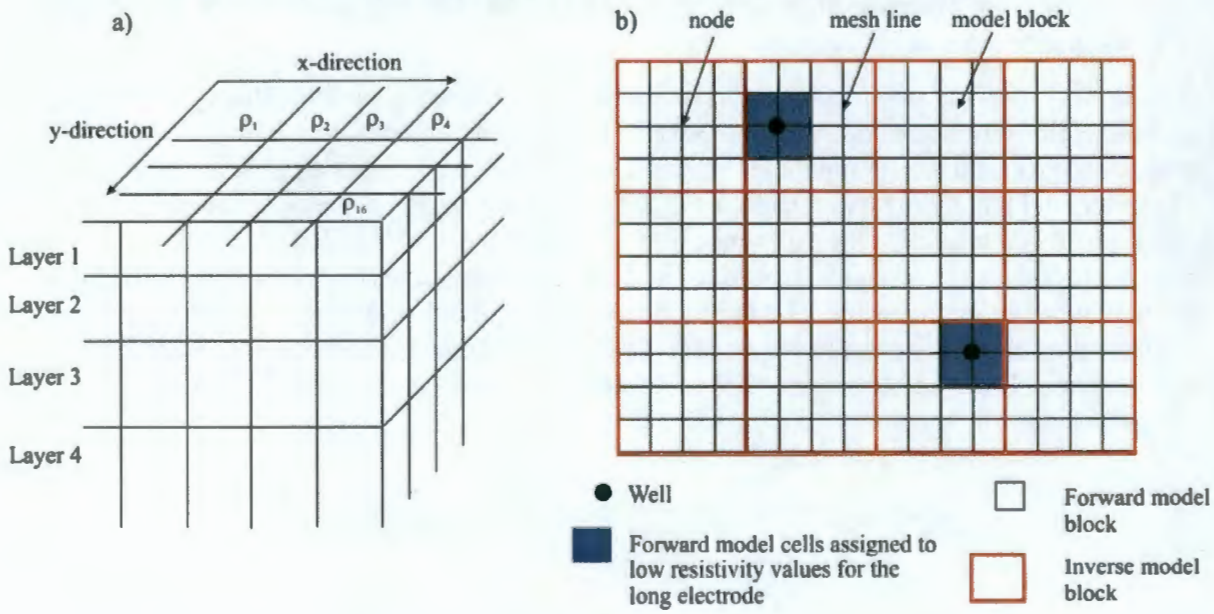

For the inversion code, the inverse mesh is separate from the forward mesh when using the long electrode module.

Accommodating long electrodes in commercial resistivity modeling codes can be accomplished easily by taking advantage of the existing code structure. Although, formally, the long electrodes act as linear sources and receivers, they can be modeled with a point source on the surface and by assigning to the long electrode's position a series of very conductive cells, say 0.01 ohm-m to simulate a metallic well. The current source is located at a node and the adjacent four cells are assigned the low resistivity values (Figure B-1b). The high contrast between the well's resistivity and that of the surrounding medium can cause adverse effects in the numerical model such as accuracy and stability. In order to reduce this problem, the forward model mesh is discretized more finely relative to the inverse model mesh so that a more gradual transition of electrical resistivity occurs between the well and the host medium.

An example of the capability of the resistivity code is demonstrated by placing a single long electrode in a 100 ohm-m background. The numerical results of transfer resistance using the finite difference method are compared to an analytic solution of an infinite conductor of infinitesimal diameter. This is taken from:

- Johnston, R. H., F. N. Trofimenkoff, and J. W. Hasslett, 1987, "Resistivity response of a homogeneous earth with a finite-length contained vertical conductor," *IEEE Transactions on Geoscience and Remote Sensing*, GE-25, 414-421
- Warrick, A. W. and A. Rojano, 1999, "Effects of source cavity shape on steady, three-dimensional flow of soil gases," *Water Resources Research*, May, Volume 35, Number 5, pp. 1425-1433.

$$R = \frac{V}{I} = \frac{\rho}{4\pi b} \ln\left[\frac{\left[r^2 + b^2\right]^{0.5} + b}{\left[r^2 + b^2\right]^{0.5} - b}\right] \qquad (2)$$

where:

ρ = the resistivity of the background

b = the length of the long electrode (or well) extending from the surface of the earth

r = the distance between the center of the well and the potential measurement location.

Equation (2) can be shown to revert to the solution of a purely homogeneous half-space for $b \rightarrow 0$. For the numerical modeling, the length of the long electrode was simulated as 44 m. The transfer resistance results in Figure B-2 show that the resistivities of between 0.01 and 0.001 ohm-m assigned to the long electrode produce the most accurate results. Specifically for this example, the resistivity of 0.006 ohm-m is the most accurate with a difference of less than four percent from the analytical values for the entire distance of 1 to 50 m away from the well. The differences are likely partially due to the assumptions of the infinite conductor and infinitesimal diameter for the analytical solution compared to the finite conductor and diameter for the numerical models (Figure B-2).

Figure B-2. Numerical Model Results of a Finite Conductor of Finite Length and Finite Diameter Compared to the Analytical Solution of an Infinite Conductor of Infinitesimal Diameter.

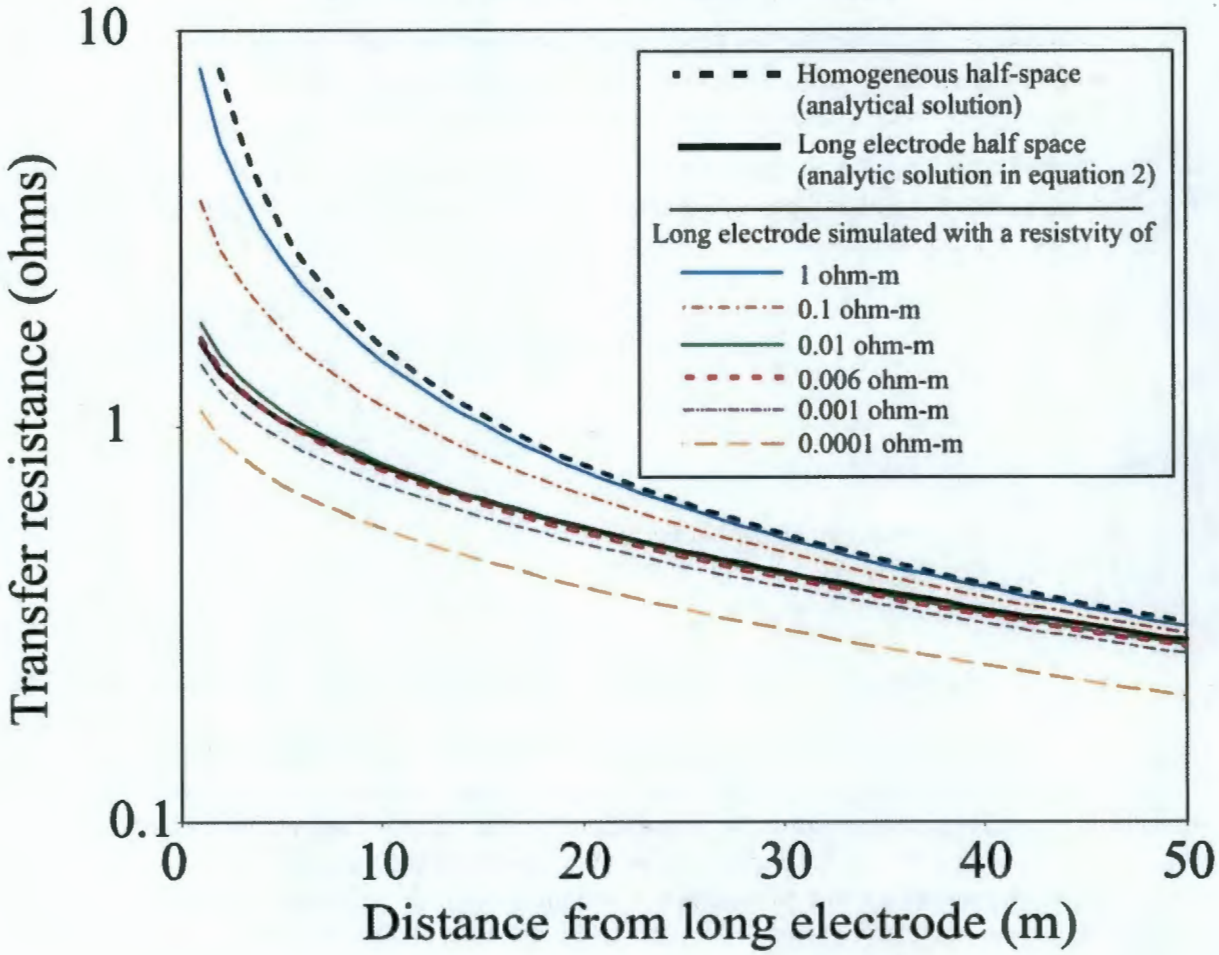

It is interesting to note that the numerical results with the lowest resistivity of 0.0001 ohm-m are very inaccurate. We suspect that the contrast between the 0.0001 ohm-m and the 100 ohm-m background (a resistivity contrast of 1:1,000,000) is too large such that the numerical method breaks down, either due to numerical round-off errors or the poor assumption of linear variation of the potential within each finite-difference cell.

The inversion of long electrode data is similar to that presented in Dahlin et al. (2002), "A 3-D resistivity investigation of a contaminated site at Lernacken, Sweden," as well as Loke et al. (2003), with either the L_2 norm smoothness-constrained least squares that aims to minimize the square of the misfit between the measured and modeled data (deGroot-Hedlin and Constable, 1990, "Occam's inversion to generate smooth, two-dimensional models from magnetotelluric data," and Ellis and Oldenburg, 1994, "Applied geophysical inversion").

$$\left(J_i^T J_i + \lambda_1 W^T W\right)\Delta r_i = J_i^T g_i - \lambda_1 W^T W r_{i-1} \tag{3}$$

or the L_1 norm that minimizes the sum of the absolute value of the misfit:

$$\left(J_i^T R_d J_i + \lambda_1 W^T R_m W\right)\Delta r_i = J_i^T R_d g_i - \lambda_1 W^T R_m W r_{i-1} \tag{4}$$

where:

G = data misfit vector containing the difference between the measured and modeled data

J = Jacobian matrix of partial derivatives

W = the roughness filter

R_d and R_m = weighting matrices to equate model misfit and model roughness

Δr_i = the change in model parameters for the ith iteration

r_i = the model parameters for the previous iteration, i

λ_i = the damping factor.

The logarithms of the model resistivity and measured apparent resistivity values are used as the model parameters and data respectively in the above equations. The long electrode module implemented in RES3D, developed by Geotomo Software allows the wells to be located at an arbitrary grid point, separate from the discretization used for the inversion model blocks (Figure B-1). The arbitrary grid modification simplifies the problem by eliminating the need to calculate the resistivity on a large number of small blocks.

B1.1 WELL-TO-WELL INVERSION EXAMPLES

The original well-to-well (WTW) inversion at the C Tank farm used the resistivity code EI3D, which has since been upgraded to accommodate large memory, multi-processor computers to EI3DCL. The EI3D code solved the WTW resistivity problem adequately, typically creating somewhat noisy results due to the incorporation of the resistivity values of the cells assigned to the well into the resistivity inversion.

The code RES3D has since been updated to conduct WTW inversion and a comparison of its strengths over EI3D is demonstrated below. Consider the following scenario: A simple target is placed in a background of 100 ohm-m. The target is 1 ohm-m and resides at the depths of 10 to 15 m below ground surface. The larger domain is 60 by 60 m and the target is 15 by 15 m placed slightly off center. The pole-pole array is used for all simulations. The results of first running the forward simulation to obtain the potential measurements then inverting the potentials to calculate the resistivity distribution is shown in Figure B-3. The figure compares the results of

RES3D and EI3D, with RES3D producing an image more similar to the initial conditions than EI3D. The EI3D results are not necessarily incorrect, but the noise surrounding the target makes the subsurface more difficult to interpret. In contrast, the target identified by RES3D is more coherent.

Figure B-3. Comparison of WTW Inversion with RES3DINVx64 (RES3D) and EarthImager3D (EI3D).

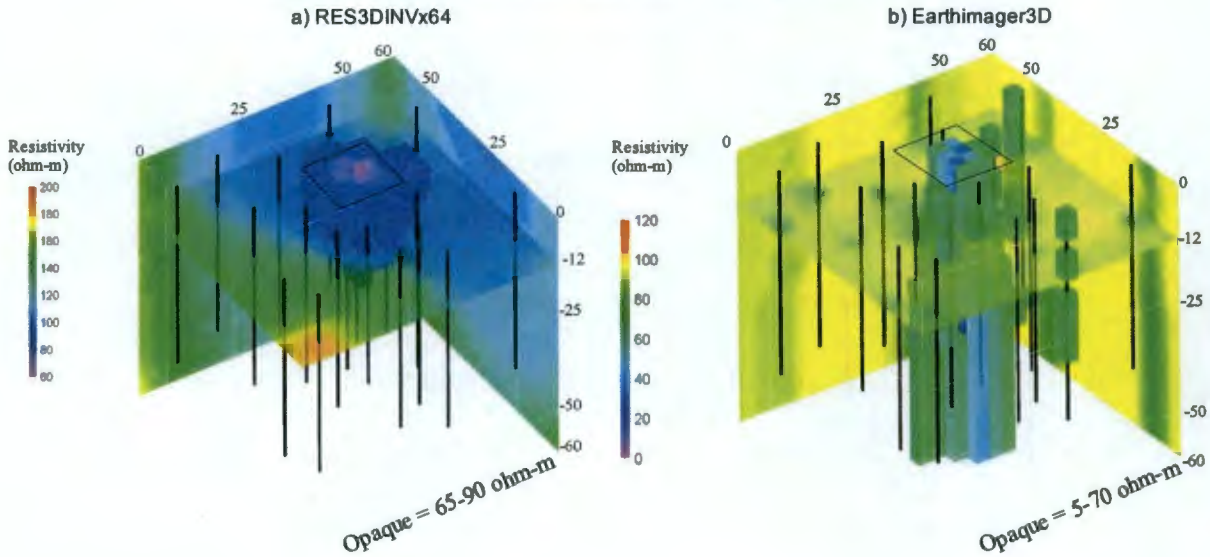

An example of the WTW inversion method and the advantage of using wells as electrodes in infrastructure-rich areas, consider the same scenario as above, but comparing STS with WTW. Figure B-4a shows the inversion results for surface electrodes only using RES3D. The surface electrodes are evenly spaced 5m apart over the entire domain for a total of 36 electrodes and 630 measured potential values. In the figure, the higher resistivity values are peeled away to reveal the lowest values that range from 50-80 ohm-m. These values were chosen such that the footprint of the inverted target matched the footprint of the original target. For reference, a transparent horizontal color contoured layer is placed at a depth of 12 m, through the center of the original target. The inverted target matches the footprint of the original target quite well with some vertical smearing that is common with this type of reconstruction.

Figure B-4b shows the inversion results from a similar circumstance but with the use of 20 long electrodes and no surface electrodes. The parameters of the long electrodes are the same as that in Figure B-2. The density of long electrodes (200 m^2/electrode) for the model were meant to replicate that of a typical tank farm (~188 m^2/well) and the electrode arrangement placed two electrodes through the target. The inversion results show a high propensity for the long electrode technique to replicate the target but with an elevated resistivity distribution compared to Figure B-4a. Additionally, the vertical distribution of the target is funnel shaped where the majority of the low resistivity values are at the surface. We surmise that the finite conductivity value used for the long electrode causes much of the current density to be concentrated nearer the

surface. This fact will likely cause a loss of vertical resolution when using the long electrode technique in the field.

Figures B-4c and B-4d show a repeat of the previous two models with the exception of a 0.25 m thick, high conductivity layer (0.01 ohm-m) at a depth of 1 m. The simulated infrastructure was slightly higher in resistivity than the well to replicate the fact that piping and tanks would never actually touch a well. The inversion with surface electrodes shows a thin low resistivity layer that obliterates the target below it, making the original target indistinguishable. Although only the lowest resistivity values are shown in Figure B-4c, a cycling through the complete set of data fails to reveal any information about the original target's whereabouts. The use of long electrodes in Figure B-4d overcomes the conductive surface layer issue and makes a good attempt to reproduce the lateral position of the target. The long electrode results with a surface layer lowers the overall resistivity values of the target and background compared to Figures B-4a and B-4b. Therefore, limitations can be expected with the long electrode technique when applying petrophysical models for estimations of moisture content or salt concentration, as the resistivity of the inverted target will depend on the amount of infrastructure and number of wells. The long electrode method should be applied more as a target recognition technique.

Other configurations of the simple target using the WTW method were tested in anticipation of conditions in the C tank farm. These configurations included:

- Deep target located at the depth of 60 m, below the bottom of the wells
- Shallow target at 10 m depth with water table at 75 m and using two groundwater wells in place of two vadose zone wells. Groundwater wells were placed at the periphery of the domain.

The results of these additional model examples are presented in Figure B-5 as horizontal slices of contoured resistivity values for the upper most layer, with Figure B-5a repeating the same data as Figure B-4b. Figure B-5b shows that even if the target is deeper than the wells, the imaging methodology can still see something, albeit of lower intensity than the near surface target. Additionally, the position is slightly off center and the footprint is larger than the original target. Figure B-5c shows the effects of a shallow target and water table, with two wells extending into the water table. The water table or choice of using groundwater wells has no effect on identifying the target or its position relative to the example with no water table as presented in Figure B-5a.

Figure B-4. Example Models Showing the Resistivity Inversion Results for Surface and Long Electrodes.

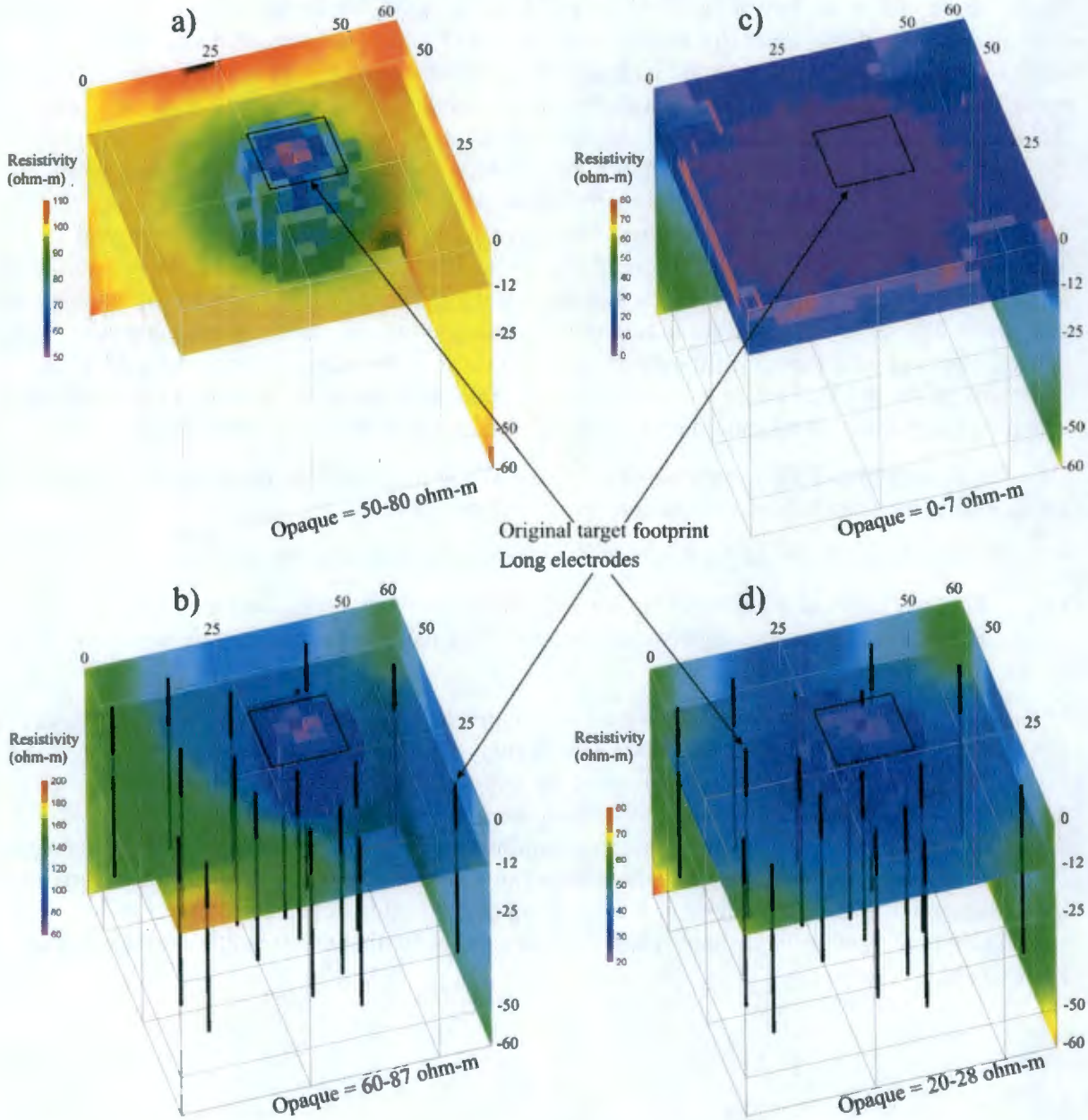

a) Surface Electrodes with Simple Target, b) Long Electrodes with Simple Target, c) Surface Electrodes with Simple Target and Conductive Surface Layer, d) Long Electrodes with Simple Target and Conductive Surface Layer. The Target Footprint is Drawn to Show the Fidelity of the Types of Electrodes to Replicate the Position of the Target.

Figure B-5. More Example Models Showing the Effects of Target Geometry and a Water Table.

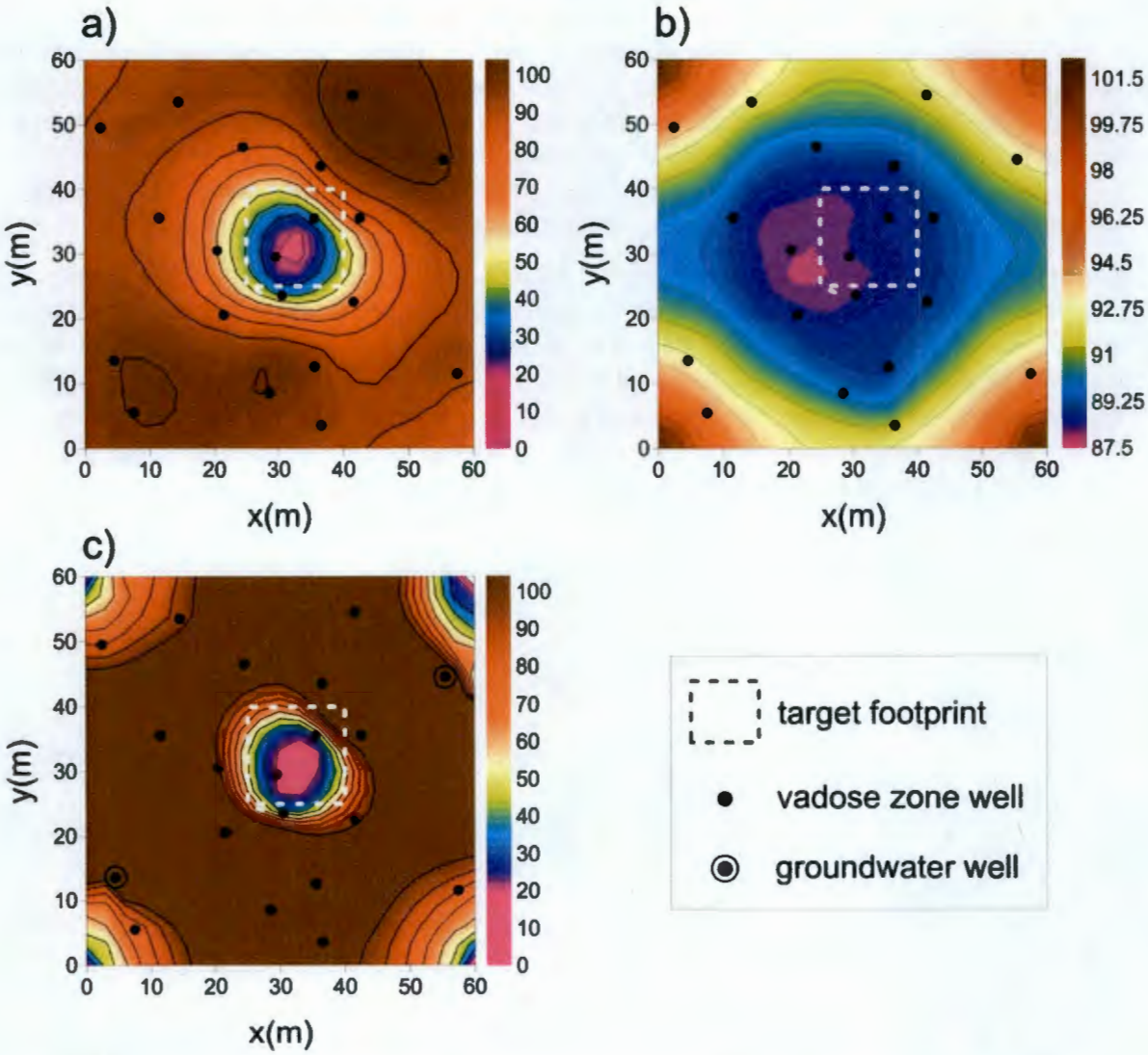

a) Long Electrodes with Simple Target, repeat of data in Figure B-4b, b) Long Electrode model with Simple Target located at 60m depth (below length of wells, c) Long electrode model with a simple target at 10 m and water table at 76m. Two wells converted to groundwater wells with lengths of 80m. The Target Footprint is Drawn to Show the Fidelity of the Types of Electrodes to Replicate the Position of the Target.

B1.2 WELL-TO-SURFACE INVERSION EXAMPLES

Incorporating surface electrodes with long electrodes has the effect of extending the measurement geometry beyond the boundaries of the well locations. To test the effectiveness of surface electrodes with wells (or well-to-surface modeling, WTS), we ran additional models, similar to those described for the WTW modeling. The WTS examples used different target

configurations, and the surface electrode distribution was similar to the arrangement at the C tank farm. The different configurations were selected to help narrow down the resolution limits of the method. The first test case used seven vadose zone wells with surface electrodes on the periphery spaced at 6 m. The target was placed in the same position as described in Figure B-4 (at 10m below the surface slightly off center). The surface electrodes were assumed to acquire data only along each individual line as if it were a profile collected on the outside of the tank farm for a surface-to-surface acquisition, with each of the wells for a WTS acquisition, and among the seven wells for a WTW acquisition. The final data file had 444 apparent resistivity measurements for the inversion model. The second test case placed the target deep in the profile, below the depth of the wells, similar to that described for Figure B-5b.

The results of the two modeling tests with WTS data are shown in Figure B-6. The first case with a shallow target shows a resulting shallow resistivity feature near the surface. The feature appears as the typical inverted cone shaped body with the largest footprint at the surface, as seen with WTW data. The results of the second example with a deep target show a resistivity feature that is much deeper. The original target was placed at a depth of 60 m but the results shows the resistivity feature much shallower at about 35 m. It appears that the WTS method can provide some depth estimation of low resistivity targets but the resolution is poor.

Figure B-6. Well-to-surface Modeling Examples with a Deep and Shallow Target.

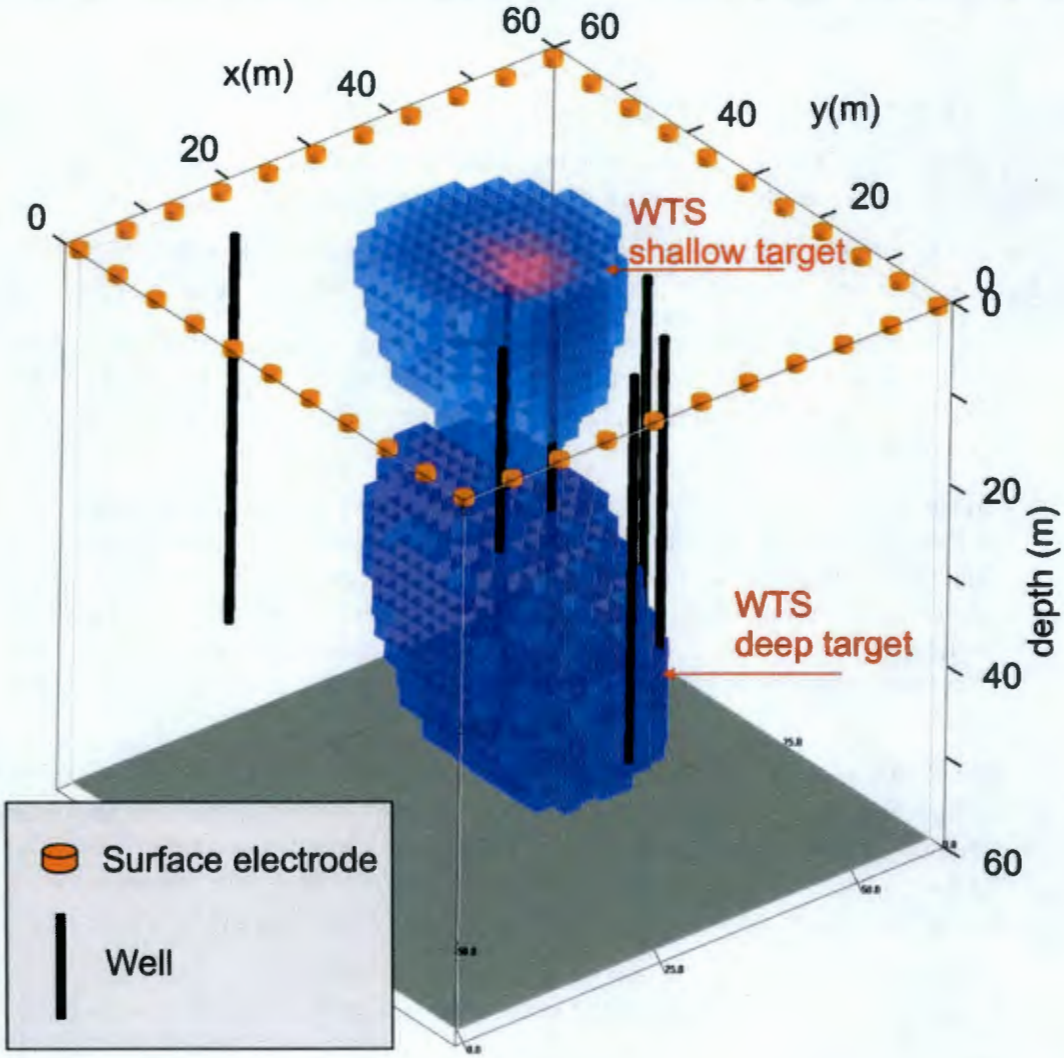

B2.0 MECHANICS OF INVERSION MODELING AND VISUALIZATION

B2.1 GEOSPATIAL DATABASE MANAGEMENT AND QUERIES

The filtered data sets from each line are used as input in the inversion modeling process. To facilitate the preparation of these data sets, all T farm resistivity data were loaded into a Microsoft Access® database. This database allows examination and evaluation of the quality control of the line layout and electrode spacing. Consistent and correct line layout and electrode coordinates are critical to the efficient functioning 3D finite difference and finite element inversion algorithms such as those used by the RES3D.

® Microsoft Access is a registered trademark of the Microsoft Corporation.

Database queries were used to extract data for several different model domains, which are then exported from the geospatial database into the ASCII format which is used by EID3 and RES3D inversion software packages.

B2.1.1 Inverse Modeling

Popular use of RES3D series of resistivity inversion codes has led both professional and academic users to regard these codes as industry standard software.

In general, the automated inversion process for RES3D proceeds as described in the following five steps. These steps are also shown graphically in a flowchart provided in Figure B-7.

1. The study site's voltage data has been measured and is discretized into grid nodes using a finite difference or finite element mesh. The meshing parameters used in either case, to design the computational grids, are dependent on electrode spacing used in site-specific data acquisition.
2. The inversion will set out to estimate the true resistivity at every grid node. An initial estimate of the subsurface properties is made based on the literal translation of the pseudo-section to a true resistivity, a constant value, or some other distribution from *a priori* information. A forward model run with these initial estimates is made to obtain the distribution of voltages in the subsurface. The root-mean-square (RMS) error is calculated between the measured voltage and the calculated voltage resulting from the forward run.
3. Based on the degree of model fit to field measurements, the initial estimate of resistivity is changed to improve the overall model fit and the forward model with the updated estimates is rerun. The iterative method linearizes a highly nonlinear problem using Newton's method. Using this method, the inversion code essentially solves the linearized problem to obtain the change in modeled resistivity (Δm) for the next iteration.
4. The resistivity model is updated using the general formula $m_{i+1} = m_i + \Delta m$, where m_{i+1} is the resistivity in a model cell at the next iteration, and the m_i is the current value.
5. Steps 3 and 4 are repeated until the RMS error change between successive iterations reaches an acceptable level.

Figure B-7. Flowchart of the Resistivity Inversion Process.

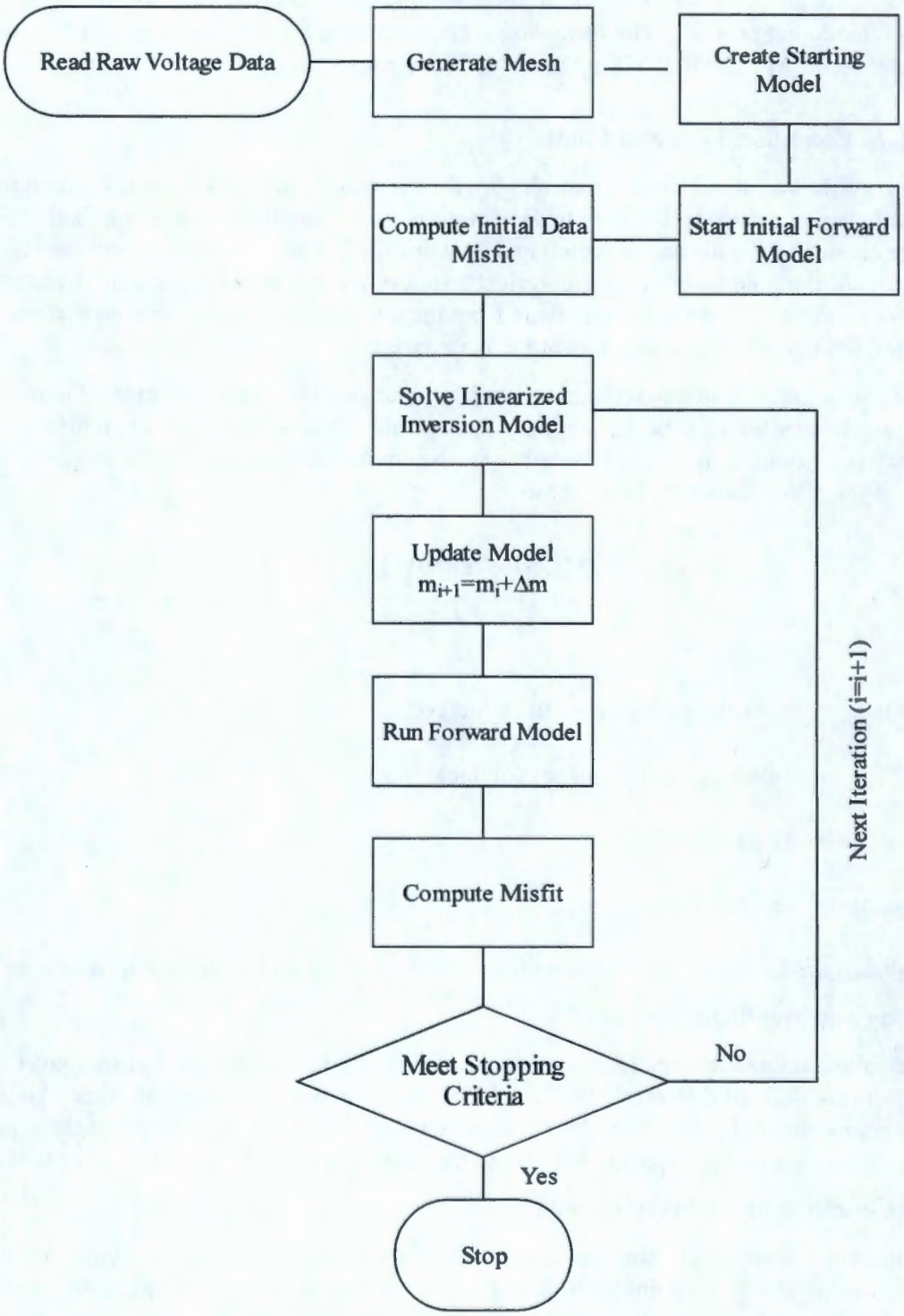

B2.1.2 Inversion Parameters

Inversion software use a series of user defined parameters to control the direction of the inversion modeling process. The following section contains a brief description of the inversion parameters used with the RES3D inversion software package.

Boundary Condition Type and Limit

The core mesh is a finite difference mesh with the same domain limits set to the maximum distance between electrodes. The boundary mesh is a continuum of the core mesh at some distance outside of the measured region and contains the boundary condition and the remote electrodes for the pole-pole array. Numerical artifacts in the core mesh are minimized when the boundary condition is set far enough away from the current sources and sinks so that the simulated field gradients are constant at the boundaries.

RES3D uses a homogeneous Neumann boundary condition (i.e., specified current density) for the surface layer which has no current flow through air. This is equivalent to an insulating boundary condition. Equation (5) describes the Neumann boundary condition as applied to the surface layer of the resistivity inverse model:

$$\rho^{-1}(s)\eta \cdot \nabla\Psi = J(s) \tag{5}$$

Where:

P = resistivity of the area to be imaged

Ψ = electrical potential (i.e. voltage)

S = core mesh area

J(s) = current density.

The value of the Dirichlet boundary condition for the bottom and sides is proprietary for RES3D.

Damping and Stabilizing Factors

The damping factors for RES3D include values for the initial, minimum, and first layer. These parameters are defined differently than the EI3D code and the exact implementation of these factors is proprietary (Loke, 2006, Personal communication via email.). Each of these parameters can be automatically optimized by RES3D so that a minimum RMS model fit error is achieved.

Initial Condition of the Inverse Model

An initial value is needed to start the calculation of the partial differential equation of the predicted value at a given point in the domain of the solution. For the T tank farm resistivity inverse model, the starting value was a homogenous solid earth set to the average apparent resistivity of the measured data.

Inverse Modeling Methodology

RES3D supports the L_2 normalized damped least-squares inverse objective function (Equation (3). Compared to the damped least squares method with no normalization or with L_1 normalization (or robust inverse modeling), the L_2 normalization is optimal at resolving naturally smooth varying electrical properties as expected for conductive plumes and most hydrologic problems.

Refer to:

- Rucker, D. F., M. Loke, G. Noonan, and M. Levitt, 2010, "Electrical Resistivity Characterization of an Industrial Site using Long Electrodes," *Geophysics*, Volume 75 (4): WA95-WA104.
- Dahlin, T., and B. Zhou, 2004, "A numerical comparison of 2D resistivity imaging with 10 electrode arrays," *Geophysical Prospecting*, Volume 52: 379-398.
- Loke, M. H., I. Acworth, and T. Dahlin, 2003, "A comparison of smooth and blocky inversion methods in 2D electrical imaging surveys," *Exploration Geophysics*, Volume 34: 182-187.
- deGroot-Hedlin, C., and S. Constable, 2004, "Inversion of magnetotelluric data for 2D structure with sharp resistivity contrasts," *Geophysics*, Volume 69(1): 78-86.
- deGroot-Hedlin, C., and S. Constable, 1990, "Occam's inversion to generate smooth, two-dimensional models from magnetotelluric data," *Geophysics* Volume 55(12): 1613-1624.

The L_2 normalization objective function is less likely to over fit smooth field measured data, in theory, reflecting a closer representation of the true conductive plume boundaries (deGroot-Hedlin and Constable 1990).

hydroGEOPHYSICS, Inc. uses the pole–pole electrode configuration due to its high signal strength at the deepest exploration depths relative to other array types, while collecting the widest horizontal coverage for a given array length (Robain et al. 1999, "The location of infinite electrodes in pole-pole electrical surveys: Consequences for 2D imaging"). The L_2 norm also appears to work well in conjunction with the pole-pole array (deGroot-Hedlin and Constable 1990).

Inverse Modeling Stop Criteria

The RMS error used in RES3D is defined in Equation (6). When the code completes an inversion, the difference in the logarithms of the measured and calculated apparent resistivity values will be similar to the relative error.

$$RMS = \sqrt{\sum_{i=1}^{N} \frac{(\log(d_{meas}) - \log(d_{pred}))^2}{N}} \times 100 \qquad (6)$$

Where:

dmeas	=	measured apparent resistivity
dpred	=	predicted apparent resistivity
N	=	the number of measurements.

If the change of RMS error between two successive inversion iterations is less than the selected value, then the inversion codes will stop. Using an RMS change stop criteria of 5 to 10 percent is recommended by Geotomo Software for field-measured surface data sets with 5 percent as the default value in both codes. In general, the percent change stop condition of 5 percent stops Geotomo Software codes as the model RMS values plateau.

Inverted Value

RES3D uses the apparent resistivity as the data input for inversion. Transfer resistance and apparent resistivity are equivalent quantities that can be converted back and forth using a geometric factor. However, the different inverted value is significant for WTW problems, where the geometric factor to convert transfer resistance to apparent resistivity does not exist. In this case, the apparent resistivity of a point electrode is assumed.

Inverted Output

The output from RES3D is in terms of X, Y, Z, and modeled resistivity.

Jacobian Matrix Calculation

The Jacobian Matrix is the matrix of all first-order partial derivatives of a vector-valued function relative to the model parameter. This calculation provides the best linear approximation to a differentiable function near a given point. The quasi-Newton or partial Jacobian Matrix calculation is a method of slightly lower accuracy, but requires less computational power. Refer to the two Geophysical Prospecting articles:

- Loke, M. H., and R. D. Barker, 1996, "Practical techniques for 3D resistivity surveys and data inversion," *Geophysical Prospecting*, 44(3): 499-523.
- McGillivray, R., and D. W. Oldenburg, 1990, "Methods for calculating Fréchet derivatives and sensitivities for the non-linear inverse problem: a comparative study," *Geophysical Prospecting*, 38(5): 499-524.

RES3D offers the option to enable the full Jacobian Matrix calculation using the Gauss-Newton method with each model update.

Model Layer Thickness Increase with Depth

The sensitivity of surface resistivity decreases with distance from the electrodes. A telescoping mesh is applied by RES3D so that lower layers are not overly resolved by the modeling process. The telescoping mesh layer thickness increases by a factor of 1.15 per layer for the T farm resistivity inverse models.

Mesh and Solver Type

RES3D incorporate finite difference and finite element mesh designs in their codes. Finite difference and finite element methods solve for electrical properties by breaking the problem area (i.e., domain) into many small elements (e.g., squares as in the finite difference or triangles, tetrahedra, etc., in finite element) and solving the equation for each element (all electrical properties are assumed constant or linearly variable within an element). The finite element method discretizes the model domain optimally for complex topographic surfaces as expected when resistivity is measured over hills and valleys. The finite difference method discretizes the model domain into block elements, which are significantly faster to compute during the inversion process. The finite difference and finite element approximation leads to an implicit set of equations that must be solved using linear algebra.

The finite difference method is used for the T farm resistivity inverse models as this is an optimal method for the Surface Geophysical Exploration (SGE) sites, which are relatively flat and involve large computationally intensive model domains. The solver type used by RES3D is proprietary, though it is very likely to be either the Cholesky Decomposition or the Conjugate Gradient solver. Both the Cholesky Decomposition and Conjugate Gradient solver are numerically equivalent, robust, and stable methods. The Cholesky Decomposition solver is generally faster and requires more memory than the Conjugate Gradient method. Refer to Golub and van Loan (2006).

Model Depth of Investigation

The deepest model layer as calculated from the array type and electrode geometry using an empirical method was proposed by Edwards (1977, "A Modified Pseudo-Section for Resistivity and IP"). RES3D use a parameter called Depth Factor. For the T farm resistivity inverse models, a value of 0.7 was used, which allowed for an appropriate model layer calculation given the array type and geometry.

Model Nodes

The number of model nodes per electrode spacing controls the density of the model mesh. A mesh with more than four nodes per electrode spacing is finer than the resolution of the resistivity method, but reduces numerical approximation errors within the mathematical model relative to coarser grids. For the T farm resistivity inverse models, the number of model nodes was set to a factor of four. Larger values directly increase the number of cells and subsequently the amount of computer memory required.

Model Resistivity Limits

The upper and lower resistivity limits are based on the reasonably expected values for a particular field area. These limits are imposed in order to reduce the chance of equivalent solutions that are outside the bounds of the true material properties. RES3D uses an upper and lower limit factor that is multiplied by the average apparent resistivity of the pseudo-section. The user manual for RES3D describes the limits as a soft constraint, which is not strictly applied.

B3.0 REFERENCES

Dahlin, T., and B. Zhou, 2004, "A numerical comparison of 2D resistivity imaging with 10 electrode arrays," *Geophysical Prospecting*, Volume 52: 379-398

Dahlin, T., C. Bernstone, and M. H. Loke, 2002, "A 3-D resistivity investigation of a contaminated site at Lernacken, Sweden," *Geophysics*, Volume 67(6): 1692-1700.

deGroot-Hedlin, C., and S. Constable, 1990, "Occam's inversion to generate smooth, two-dimensional models from magnetotelluric data," *Geophysics* Volume 55(12): 1613-1624.

deGroot-Hedlin, C., and S. Constable, 2004, "Inversion of magnetotelluric data for 2D structure with sharp resistivity contrasts," *Geophysics*, Volume 69(1): 78-86.

Dey, A., and H. F. Morrison, 1979, "Resistivity modeling for arbitrarily shaped three-dimensional structures," *Geophysics*, Volume 44(4), pp. 753-780.

Edwards, L. S., 1977, "A Modified Pseudo-Section for Resistivity and IP," *Geophysics*, Volume 43(5): 1020-036.

Ellis, R. G., and D. W. Oldenburg, 1994, "Applied geophysical inversion," *Geophysical Journal International*, 116, 5-11.

Furman, A., A. W. Warrick, and T. P. A. Ferré, 2002, "Electrical potential distributions in response to applied current in a heterogeneous subsurface, solution for circular inclusions," *Vadose Zone Journal*, 1, 273–280.

Golub, G. H., and C. F. van Loan, 2006, *Matrix Computations,* 3rd Edition, Johns Hopkins University Press, Baltimore, Maryland.

Greenhalgh, S. A., B. Zhou, M. Greenhalgh, L. Marescot, and T. Wiese, 2009, "Explicit expressions for the Fréchet derivatives in 3D anisotropic resistivity inversion," *Geophysics*, Volume 3, F31-F43.

Johnston, R. H., F. N. Trofimenkoff, and J. W. Hasslett, 1987, "Resistivity response of a homogeneous earth with a finite-length contained vertical conductor," IEEE Transactions on Geoscience and Remote Sensing, GE-25, 414-421.

Loke, 2006, Personal communication via email.

Loke, M. H., and R. D. Barker, 1996, "Practical techniques for 3D resistivity surveys and data inversion," *Geophysical Prospecting*, 44(3): 499-523.

Loke, M. H., I. Acworth, and T. Dahlin, 2003, "A comparison of smooth and blocky inversion methods in 2D electrical imaging surveys," *Exploration Geophysics*, Volume 34: 82-187.

McGillivray, R., and D. W. Oldenburg, 1990, "Methods for calculating Fréchet derivatives and sensitivities for the non-linear inverse problem: a comparative study," *Geophysical Prospecting*, 38(5): 499-524.

Pidlisecky, A., E. Haber, and R. Knight, 2007, "RESINVM3D: A 3D resistivity inversion package," *Geophysics*, 72, H1-H10.

Sasaki, Y., 1989, "Two-dimensional joint inversion of magnetotelluric and dipole-dipole resistivity data," *Geophysics*, Volume 54: 254-262.

Robain, H., Y. Albouy, M. Dabas, M. Descloitres, C. Camerlynck, P. Mechler, and A. Tabbagh, 1999, "The location of infinite electrodes in pole-pole electrical surveys: Consequences for 2D imaging," *Journal of Applied Geophysics*, Volume 41(4), pp. 313-333.

RPP-RPT-28955, 2006, *Surface Geophysical Exploration of T Tank Farm*, Prepared by hydroGEOPHYSICS and Columbia Energy and Environmental Services, Inc. for the U.S. Department of Energy, Richland, Washington.

Rucker, D. F., M. Loke, G. Noonan, and M. Levitt, 2010, "Electrical Resistivity Characterization of an Industrial Site using Long Electrodes," *Geophysics*, Volume 75 (4): WA95-WA104.

Warrick, A. W., and A. Rojano, 1999, "Effects of source cavity shape on steady, three-dimensional flow of soil gases," *Water Resources Research*, May, Volume 35, Number 5, pp. 1425-1433